UNIVERSITÀ
DI TORINO

UNIVERSITÀ DEGLI STUDI DI TORINO
Department of Molecular Biotechnology and Health Sciences

Ph.D. Program in Molecular Medicine, Cycle 34°

The adaptor proteins p130Cas and p140Cap in the control of cancer cell signaling: studies on pancreatic cancer initiation and cholesterol metabolism of breast cancer cells

Candidate: Dora Natalini

Supervisor: Prof. Paola Defilippi

Academic years of enrolment: 2018/2022

Index

1. State of the Art

1.1. The adaptor proteins p130Cas and p140Cap

Signal transduction is a cellular process that allows cells to sense stimuli and activate specific signaling molecules that propagate the information throughout the cell, ultimately leading to an appropriate cellular response. The complex and interconnected signaling pathways responsible for transmitting the received information must be tightly regulated in time and space. One of the primary proteins involved in such regulation is adaptor proteins. Specifically, they can be functionally defined as proteins devoid of any enzymatic or transcriptional activity that facilitates interactions and coordination of signaling complexes necessary to respond to a particular stimulus. Adaptor proteins contain a variety of domains or motifs that promote protein-protein interactions, and the sequence of these domains dictates the specificity in binding and the subcellular localization of the protein complexes. Therefore, adaptor proteins are positioned to regulate signaling events spatially and temporally (Flynn, 2001; Pawson & Scott, 1997).

p130Cas protein (p130 Crk-associated substrate, also known as Breast Cancer Anti-estrogen Resistance 1 [BCAR1]) and its indirect interactor p140Cap (p130Cas-associated protein or SRC Kinase Signaling Inhibitor 1 [SRCIN1]) are two adaptor proteins that participate in the control of signaling events in both physiological and pathological conditions (Cabodi, del Pilar Camacho-Leal, et al., 2010; Centonze, Natalini, Salemme, Costamagna, et al., 2021; Chapelle et al., 2019) (Camacho Leal Mdel et al., 2015). Their role has been extensively investigated in malignancies (Tornillo et al., 2014), with p130Cas being characterized as a cancer-promoting protein, whereas p140Cap acts as a tumor suppressor in specific tumors. Specifically, p140Cap has been shown to attenuate the intrinsic biological aggressiveness of breast cancer (Grasso et al., 2017), neuroblastoma (Grasso et al., 2020), and colon cancer (Damiano et al., 2010; Sharma et al., 2013) by limiting the cell migration, invasion, tumor growth, and

metastasis formation in mice (Salemme et al., 2021). In contrast, the pro-tumorigenic functions of p130Cas rely on its ability to favor the oncogenic transformation of various cell types, control the spatiotemporal regulation of focal adhesion turnover, and promote cell migration, invasion, cell-cycle progression, and mechanotransduction (Camacho Leal Mdel et al., 2015; Defilippi et al., 2006; Tornillo et al., 2014).

1.2. Protein structure and interactors of p140Cap and p130Cas

The human p140Cap is encoded by the gene SRCIN1 on chromosome 17q12. Consistent with the adaptor protein definition, p140Cap has no enzymatic or transcriptional activity and functions as a multisite docking protein characterized by conserved sequence motifs that can associate with multiple protein partners. p140Cap consists of an N-terminal tyrosine-rich region with a myristylation site, a putative actin-binding domain, a tyrosine-rich domain, two proline-rich domains (Pro1 and Pro2) that contain multiple PPxY and PxxP motives (for interaction with SH3 domains), a coil-coiled region (C1–C2), and two domains rich in charged amino acids (CH1 and CH2) (Chin et al., 2000; Di Stefano et al., 2004) (Figure 1A). Phosphorylation of p140Cap on tyrosine and, to a less extent, serine and threonine residues occur upon integrin-mediated adhesion or EGF receptor activation (Di Stefano et al., 2004). Of notice, two highly conserved sequences named “EPLYA” and “EGLYA” have been identified as the primary sites for tyrosine phosphorylation by ABL, which then allow the interaction between p140Cap and C-terminal Src kinase (Csk) (Repetto et al., 2013). The proline-rich region in the C-terminus of p140Cap was shown to directly associate with the SH3 domain of Src (Di Stefano et al., 2007). Besides Src and Csk, p140Cap binds to Beta-catenin, Vinexin, Cortactin, and EB3. Interatomic studies performed on mice show that p140Cap might associate with PPP1R9B (protein phosphatase one regulatory subunit 9B), SNCA (synuclein, alpha), YWHAE (tyrosine 3-monooxygenase/tryptophan 5-monooxygenase activation protein), LNX1 (ligand of numb-protein X1) and AGAP2 (ArfGAP with GTPase domain). Moreover, p140Cap was also identified in the interactome of NUFIP1 (nuclear fragile X mental retardation protein-interacting protein), BCAS4 (breast carcinoma amplified sequence 4), and ESR2 (estrogen receptor 2) from human samples (Salemme et al., 2021). Of note, p140Cap was initially identified as an indirect interactor of p130Cas, a major Src-binding protein, through its C-terminal domain (Di Stefano et al., 2004).

p130Cas is encoded by the gene BCAR1 on the negative strand of region q of chromosome 16. It is a member of the Cas (Crk-associated substrate) family that includes four other adaptor proteins: Nedd9 (Neural precursor cell expressed, developmentally downregulated 9), Human enhancer of filamentation-1 (HEF-1), EFS (Embryonal Fyn-associated substrate), and CASS4 (Cas scaffolding protein family member 4) (Nikonova et al., 2014). These proteins share similar modular structures characterized by interaction domains and various tyrosine and serine phosphorylation motifs. Cas proteins regulate the magnitude and duration of signaling cascades involved in several biological processes, including cell adhesion, spreading, migration, invasion, and proliferation. The protein structure of p130Cas features an amino (N)-terminal Src-homology 3 (SH3) domain, a proline-rich region, an adjacent substrate-binding domain characterized by fifteen YxxP motifs, a serine-rich part, a carboxy (C)-terminal region domain containing the conserved CCH (C-terminal CAS-family homology) domain (Figure 1B)(Defilippi et al., 2006). Like p140Cap, p130Cas lacks any enzymatic or transcriptional activity; however, the proline-rich region, the SH3 domain, and the extensive phosphorylation in tyrosines and serines provide docking sites for a variety of interactor proteins. The signals that induce tyrosine phosphorylation on p130Cas are integrin-mediated adhesion, receptor tyrosine kinase (RTK) or chemokine receptor activation, and hypoxia. Thus, phosphorylated tyrosines can associate with several effector molecules, including the non-receptor focal adhesion kinase (FAK), SRC family kinases (SFKs), Abelson kinase (ABL), and several phosphatases, leading to the formation of a molecular hub capable of tuning specific cell functions(Cabodi, del Pilar Camacho-Leal, et al., 2010). Specifically, it has been shown that SFKs bind the (C)-term domain of p130Cas, whereas phosphorylation of YxxP motifs by SFKs mediates the binding to CRK, CRK-L, CRKII, and NCK (Schlaepfer et al., 1997). A detailed description of direct

and indirect interactors is provided elsewhere (Cabodi, del Pilar Camacho-Leal, et al., 2010; Camacho Leal Mdel et al., 2015; Di Stefano et al., 2011).

Figure 1

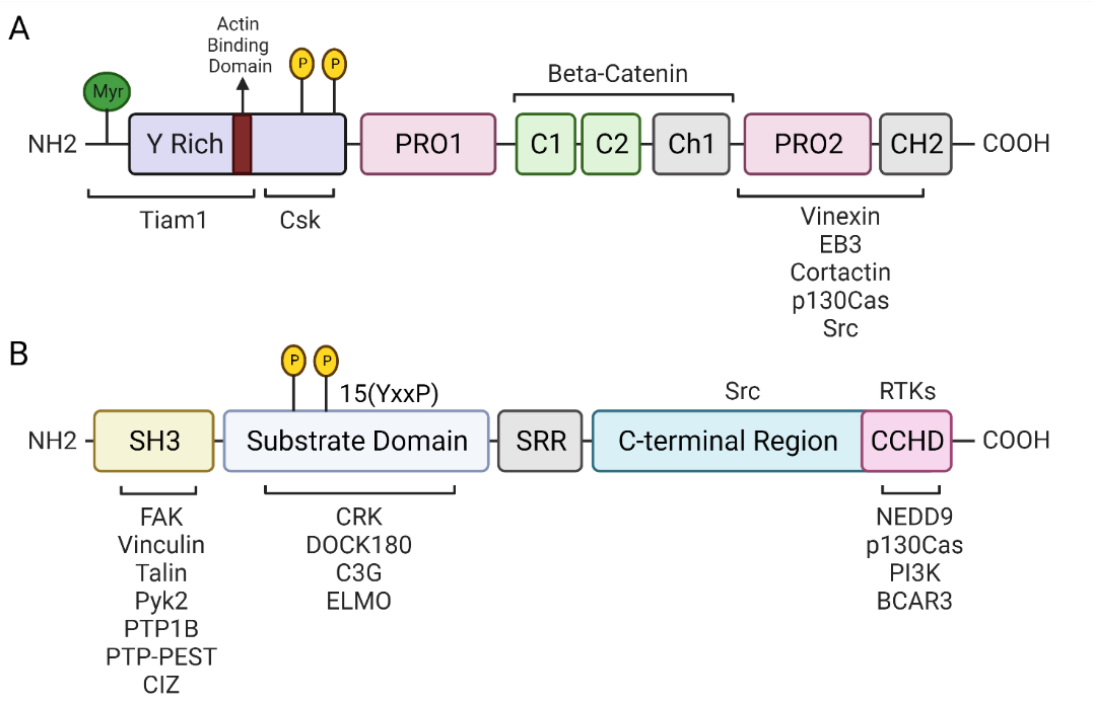

Figure 1. p140Cap/SRCIN1 and p130Cas/BCAR1 protein structures and known interactors. (A) p140Cap consists of an N-terminal tyrosine-rich region with a myristylation site, a putative actin-binding domain, proline-rich regions (PRO1 and PRO2), coil-coiled regions (C1 and C2), and CH1 and CH2 - domains rich in charged amino acids. (B) p130Cas protein contains an amino (N)-terminal Src-homology 3 (SH3) domain, a proline-rich region, a substrate-binding domain characterized by fifteen YxxP motifs, a serine-rich part (SRR), a carboxy (C)-terminal region domain containing the C-terminal CAS-family homology domain (CCHD). The known interactors are reported above or below the identified interacting domains.

1.3. Expression of p130Cas and p140Cap in physiology and cancer

p140Cap expression is highly tissue-specific. Indeed, it is mainly expressed in neurons, specifically in their dendritic spines. It primarily functions as a scaffold protein of the post-synaptic density (PSD), a thick electron-dense membrane-associated protein complex involved in signaling regulation and remodeling of actin dynamics (Jaworski et al., 2009). In this context, p140Cap is crucial in synaptogenesis, synaptic transmission, and synaptic plasticity (Jaworski et al., 2009; Repetto et al., 2014; Tomasoni et al., 2013). Moreover, p140Cap is present in epithelial-rich tissues, including the lung, testis, heart, kidney, and mammary glands, although to a lesser extent than in neuronal tissues (Di Stefano et al., 2004). In normal human mammary glands, the protein is in alveolar luminal cells, although its physiological role has yet to be identified (Damiano et al., 2010). In addition, IHC staining of the Wistar rat pancreas revealed that p140Cap is enriched in the beta cells, forming a cytoplasmic granular pattern (Yamauchi et al., 2013). The evidence on the regulation of p140Cap gene expression is limited. Still, we know that amplification or rearrangements of the chromosomal region containing the SRCIN1 gene can occur in cancer (Salemme et al., 2021). Notably, p140Cap expression correlates with a good prognosis in breast cancer and neuroblastoma. Breast tumors with a high proliferative phenotype (indicted by Ki67 positivity) tend to lose p140Cap expression, suggesting an inverse correlation with malignancy (Damiano et al., 2010). Notably, high p140Cap protein level in invasive breast cancer is associated with good prognosis markers, such as negative lymph node status, estrogen receptor (ER) and progesterone receptor (PR)-positive status, small tumor size, low grade, and low proliferative and ERBB2-positive status. The SRCIN1 gene is frequently co-amplified with ERBB2 due to the chromosomal rearrangement of the ERBB2 amplicon. A study using BAC array Comparative Genomic Hybridization revealed that the SRCIN1 gene is altered in 70% of ERBB2-amplified tumors, exhibiting a copy number gain in 61.5% of cases (Grasso et al., 2017). The same study found that a

high protein level of p140Cap in ERBB2-amplified tumors is associated with a significantly lower probability of developing a distant event and death from breast cancer. Moreover, p140Cap mRNA expression correlates with a good outcome in neuroblastoma patients in terms of survival and event-free survival, providing a new independent prognostic marker (Grasso et al., 2020). The SRCIN1 gene status is deregulated in some NB tumors. Indeed, the SRCIN1 gene spans a chromosomal region frequently involved in genetic abnormalities in NB, including the 17q gain. Grasso S. and coworkers assessed the SRCIN1 gene status by high-resolution oligonucleotide a-CGH and SNP-array on 225 NB primary tumors of all stages with 17q gain. In four NB tumors, SRCIN1 was hemizygously deleted; in three was subjected to copy-neutral loss of heterozygosity, and in ten was disrupted because located at the breakpoint of the 17q segment involved in the generation of 17q gain. Many studies report the post-transcriptional control of p140Cap through micro RNAs (miRNAs) in different malignancies, including colorectal, gastric, pancreatic, breast, ovarian, lung cancers, hepatocellular and cervical carcinomas (Salemme et al., 2021). The direct targeting of p140Cap by several miRNAs has been validated in cancer cell lines, leading to enhanced tumor features such as proliferation, migration, invasion, and angiogenesis.

Contrary to p140Cap, p130Cas is ubiquitously expressed and plays a crucial role in mouse development. Indeed, p130Cas-deficient mice die at embryonic day 12.5 due to massive cardiac and circulatory dysfunction, indicating that this protein is necessary for the early developmental processes (Honda et al., 1998).
The relevance of p130Cas in cancer has been extensively demonstrated. Indeed, p130Cas expression is often de-regulated in cancer, contributing to cellular transformation and cancer progression. The overexpression may result from gene amplification, transcription up-regulation, or changes in protein stability, although the exact mechanisms need to be clarified. p130Cas overexpression has been detected in the human breast, prostate, ovarian, lung, colorectal,

pancreatic, and hepatocellular carcinoma, as well as in glioma, melanoma, anaplastic large cell lymphoma, and chronic myelogenous leukemia (Tikhmyanova et al., 2010). For instance, In ERBB2-amplified-breast cancer, high p130Cas levels correlate with poor prognosis and enhanced metastasis formation (Tornillo et al., 2011). Conversely, downregulating p130Cas expression levels in several cancer cells, including breast, prostate, and ovarian cancer, leads to tumor growth inhibition (Cabodi, Tinnirello, e al., 2010; Dai et al., 2011; Nick et al., 2011).

1.4. Involvement of p140Cap/SRCIN1 and p130Cas/BCAR1 in cancer cell signaling

p140Cap is implicated in regulating various signaling pathways in BC cells. p140Cap has been initially described as a crucial inhibitor of the Src kinase activity, through the interaction with its negative regulator Csk, upon extracellular cell-matrix adhesion and EGFR activation (Di Stefano et al., 2007). The binding between p140Cap and Csk triggers Csk activation, which subsequently phosphorylates the C-terminal inhibitory tyrosine residue 527 of Src. This event will enable the association between the C-terminal and the N-terminal SH2 domains of Src, promoting a conformational change that closes the molecule to an inactive state (Koegl et al., 1995). By doing so, p140Cap inhibits the downstream Src-dependent tyrosine 925 phosphorylation of FAK, impairing the stability of Fak and Src associations and reducing the integrin-dependent phosphorylation of p130Cas (Di Stefano et al., 2007).

In addition, p140Cap negatively affects the Rac1 GTPase activity (Grasso et al., 2017). Specifically, ERBB2-positive cancer cells that express p140Cap have reduced activity of Rac1 and its GEF Tiam1. At the molecular level, the N-terminal domain of p140Cap is sufficient for the association of Tiam1, causing reduced Tiam1 activity. Moreover, p140Cap forms a molecular complex with Tiam1 and E-cadherin, causing the redistribution of Tiam1 along the apicobasal junctional axis (Chapelle et al., 2020). Of note, in a large cohort of ERBB-2 positive BC patients, high levels of SRCIN1 expression positively correlate with increased survival in patients with high Tiam1 gene expression (Chapelle et al., 2020). E-cadherin levels are strongly down-regulated during the epithelial-to-mesenchymal transition (EMT), a cellular process necessary for metastasis formation (Bill & Christofori, 2015; Lamouille et al., 2014). In this regard, p140Cap promotes increased E-cadherin mRNA levels and higher distribution and stabilization of E-cadherin at the cancer cell surface. Therefore, p140Cap stabilizes adherens junctions and inhibits EGFR and Ras signaling through the dual control of Src and

Ras activities, thus affecting crucial cancer properties such as cell invasion and tumor growth (Damiano et al., 2010). Furthermore, p140Cap exerts an inhibitory effect on counteracting the EMT invasive program of ERBB2-positive tumors by downregulating the EMT transcription factors Snail, Slug, Zeb1, and the mesenchymal cell-cell adhesion protein N-cadherin (Grasso et al., 2017).

In neuroblastoma (NB) cell lines, p140Cap dampens Src kinase activation, tyrosine phosphorylation of p130Cas, and phosphorylation of STAT3 Tyr 705 and its upstream tyrosine kinase JAK2 (Grasso et al., 2020). Consistently, silencing of endogenous p140Cap in the neuroblastoma cell line SH-SY-5Y leads to the increased phosphorylation of Src and STAT3. These molecular alterations reduce *in vitro* anchorage-independent growth and cell migration, *in vivo* tumor growth, and spontaneous lung metastasis formation. p140Cap also increases the sensitivity of neuroblastoma cells to doxorubicin and etoposide treatment, two drugs used in NB first-line treatments. These drugs target the process of DNA replication. In line with this, p140Cap-expressing NB cells harbor a significant increase in the DNA marker phosphorylated histone H2AX gamma. Moreover, the sensitivity of NB cells to doxorubicin and etoposide is enhanced when combined with Saracatinib and Sugen, two well-known Src inhibitors. The axis FAK/Src/Paxillin is a marker of unfavorable prognosis for human NB patients and represents a promising therapeutic target (Kratimenos et al., 2017; Navarra et al., 2010; Radi et al., 2011). In this regard, p140Cap-expressing NB cells are more sensitive to combined treatment with chemotherapy drugs and Src inhibitors (Grasso et al., 2020).

p130Cas is a cytoplasmic protein; however, upon extracellular matrix attachment and integrin engagement, it migrates to focal adhesion thanks to tyrosine phosphorylation in the substrate domain and the association of the SH3 domain of p130Cas with FAK or vinculin. p130Cas has mechanosensory properties since it can sense and respond to mechanical stimuli. Indeed, mechanical stress

increase tyrosine phosphorylation in the substrate domain of p130Cas, promoting the association with signaling molecules such as the Crk/C3G complex, leading to the subsequent activation of Src, Rap1, Rac1, ERK, and other signaling pathways (Daday et al., 2022; Miyazaki et al., 2019; Sawada et al., 2006).

In the context of ERBB2-positive BC cells, p130Cas promotes and amplifies the oncogenic signaling driven by ERBB2. Indeed, concomitant p130Cas over-expression and ErbB2 activation promote PI3K/Akt and Erk1/2 MAPK signaling pathways, which are necessary to induce the invasion of mammary acini (Tornillo et al., 2011). Erk1/2 MAPK and PI3K/Akt signaling pathways trigger the invasive phenotype through distinct downstream mechanisms involving mTOR/p70S6K and Rac1 activation, respectively. Moreover, p130Cas contributes to the ERBB2-positive BC cell invasion through increased MMP9 activity (Cabodi, Tinnirello, et al., 2010). The molecular mechanism underlying the pro-tumorigenic role of p130Cas in ERBB2-driven breast cancer relies on its ability to promote a molecular complex comprising ErbB2, c-Src, and FAK, thus supporting cell invasion and proliferation. In addition, p130Cas can stabilize ErbB2 by reducing its autophagy-dependent degradation (Bisaro et al., 2016).

In pancreatic cancer, p130Cas tyrosine phosphorylation and the subsequent association with Nck1 are detrimental to the activation of Rap1 downstream of EGFR. Nevertheless, the activation of the p130Cas/Rap1 axis is relevant for EGFR-induced metastasis without impacting the primary tumor growth (Huang et al., 2012).

2. Aims of the Research

Here, I will present the research work conducted during my Ph.D. program, which can be divided into two fundamental projects regarding the study of the adaptor proteins p130Cas and p140Cap in two different cancers: pancreatic adenocarcinoma and breast cancer.

This thesis has two fundamental aims:

1) Understand the role of the adaptor protein p130Cas in controlling oncogenic signaling events underlying pancreatic cancer development

2) Dissect the contribution of p140Cap in the modulation of cholesterol metabolism in breast cancer cells.

3. The role of p130Cas in Acinar to Ductal Metaplasia

Concerning the work on p130Cas in PDAC initiation, I will focus on the generation of pre-clinical mouse models and the cell signaling studies that led to the identification of a new signaling pathway controlling oncogenic KRAS-induced pancreatic adenocarcinoma initiation. This research work culminated with the publication of an original co-authored article in the journal Gastroenterology (Costamagna et al., 2022).

This work aims to define the role of the adaptor protein p130Cas/BCAR1 in pancreatic cancer development. The research objectives are the following:

1. Develop mouse models of PDAC suitable for investigating the role of p130Cas in Kras-induced acinar metaplasia.
2. Investigate the influence of p130Cas in the signaling events underlying Kras-induced ADM by using isolated pancreatic acini.

3.1. Introduction

Pancreatic ductal adenocarcinoma (PDAC) is one of the most lethal neoplasms worldwide, accounting for 8.2% of all cancer deaths with a 5-year relative survival of 11.5% (Bailey et al., 2014; *Cancer Stat Facts: Pancreatic Cancer*) The most common genetic alteration is the Kras mutational activation, that occurs in approximately 85% of patients, in the earliest precancerous lesions. Because the direct targeting of Kras is complex, understanding the initial steps that lead to pancreatic cancer initiation is crucial for identifying early detection markers and developing new therapeutic approaches. Kras-driven PDAC can arise from acinar cells undergoing a transdifferentiation process called acinar to ductal metaplasia (ADM) (Bailey et al., 2014; Storz, 2017; Storz & Crawford, 2020). Genome-Wide Association Studies (GWAS) have identified BCAR1 as a new pancreatic cancer susceptibility gene (Childs et al., 2015; Gong et al., 2018; Wolpin et al., 2014). In pancreatic cancer cell lines, p130Cas was identified as a mutant Kras-synthetic lethal interactor, and suppression of BCAR1 sensitizes pancreatic cancer cells to ERK inhibition via the DOCK1–RAC1–β-catenin axis and Myc regulation (Waters et al., 2021). However, the role of p130Cas in PDAC initiation is unknown.

3.2. Results

p130Cas is overexpressed in ADM and preneoplastic lesions in preclinical models of KRAS-induced PDAC

To investigate the role of p130Cas during Kras-dependent pancreatic tumorigenesis, we took advantage of Pdx^{Cre}; $Kras^{G12D}$ and Pdx^{Cre}; $Kras^{G12D}$; $Trp53^{R172H}$ pancreatic cancer mouse models (referred to from now on as $Kras^{G12D}$ and $Kras^{G12D}$; $Trp53^{R172H}$) (Hingorani et al., 2003; Hingorani et al., 2005). Notably, p130Cas expression was very low or undetectable in normal pancreatic acini and ducts (Figure 2A, left panel), whereas it was overexpressed in high-grade lesions in both murine models. p130Cas staining intensity increased in low-grade ADM and pancreatic intraepithelial neoplasia (PanIN)1–2 lesions of 2- and 4-month-old $Kras^{G12D}$ mice (Figure 2A, central panels), as well as in high-grade PanIN3 lesions and PDAC areas of $Kras^{G12D}$; $Trp53^{R172H}$ mice (Figure 2A, right panel), but remained low or undetectable in the adjacent stroma and immune cells. However, p130Cas expression did not increase further from ADM to PDAC lesions, but the areas with high p130Cas positivity increased parallel to tumor progression (Figures 2B and C). These data suggest that p130Cas overexpression might play a crucial role in Kras-induced ADM and the formation of preneoplastic lesions.

Generation and characterization of conditional p130Cas KO PDAC mouse model

To further investigate if loss of p130Cas could inhibit $Kras^{G12D}$-driven ADM, we generated mice that specifically lack p130Cas expression in the pancreatic epithelium, crossing the $Kras^{G12D}$ model with mice carrying floxed p130Cas alleles ($p130Cas^{fl/fl}$)(Camacho Leal et al., 2018). By employing a conditional approach to specifically delete p130Cas in the pancreatic epithelium, we circumvent the embryonic lethality of germ-line p130Cas KO (Honda et al., 1998). To exclude gross pancreatic abnormalities in mice lacking p130Cas, pancreata from Pdx^{Cre}; $p130Cas^{KO}$ mice were histologically examined. These pancreata appeared normal, indicating that p130Cas was dispensable for pancreas development (Figure 2D).

Suppression of p130Cas protein expression in the pancreatic epithelium was confirmed by Western blot analysis (Figure 2E). Pdx^{Cre}; $p130Cas^{KO}$ mice were viable and born at the expected Mendelian ratio (Figure 2F).

Figure 2

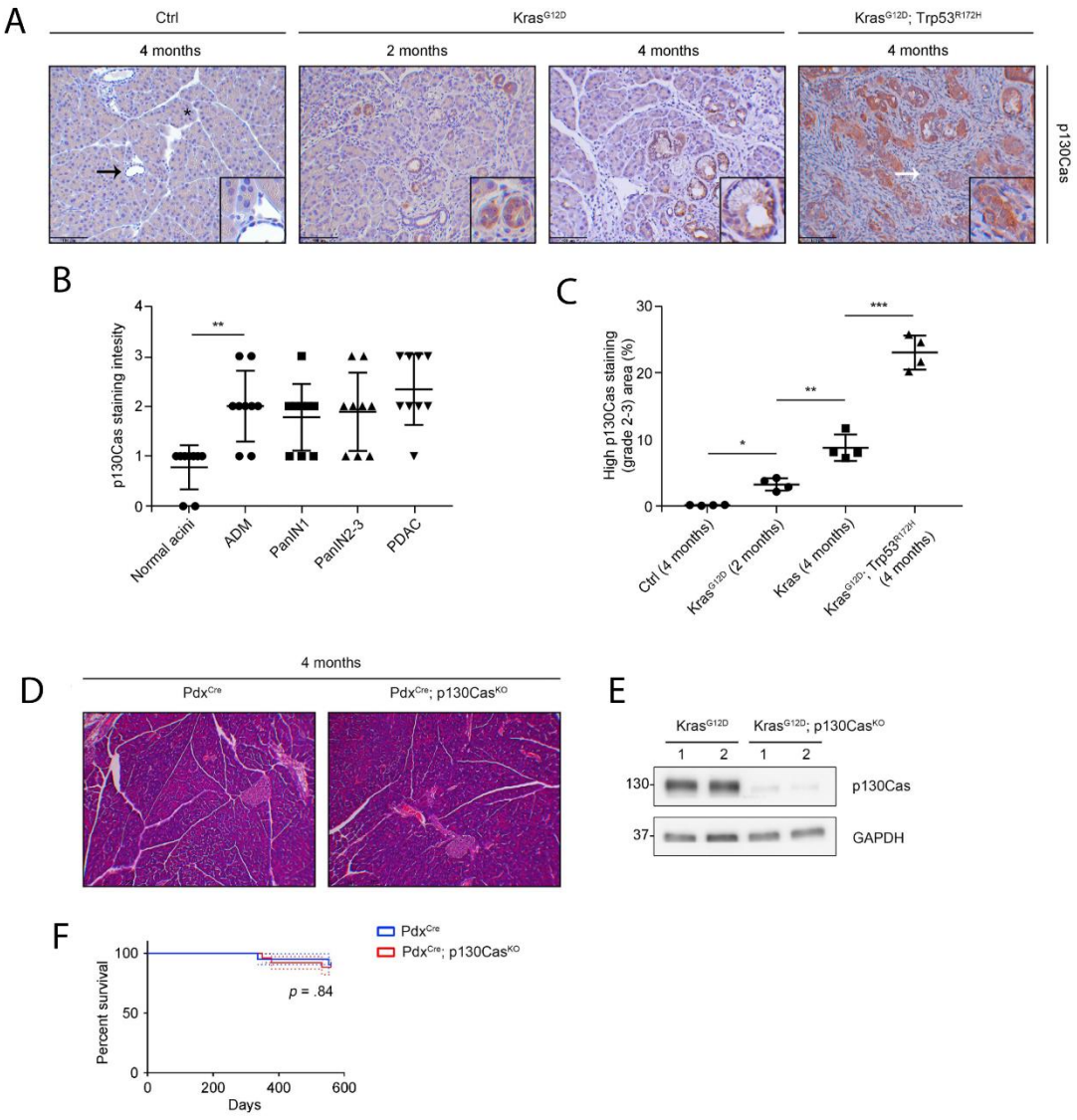

Figure 2. p130Cas expression in the pancreata of mice models for KRAS-induced PDAC and generation of the conditional p130Cas KO. (A) Immunohistochemical (IHC) staining for p130Cas in pancreatic tissue from control mice (PdxCre; Kraswt/wt), 2- and 4-month-old KrasG12D mice, and 4-month-old KrasG12D; Trp53R172H mice. Asterisks indicate normal pancreatic acinar tissue. Black arrows indicate normal pancreatic duct morphology. White arrows indicate stromal components. (B)

Quantification of p130Cas IHC staining intensity, ranging from absent (0) to highest (3). (C) Quantification of the area with high (grade 2–3) p130Cas staining.

p130Cas is crucial for Kras-mediated ADM in a cell-autonomous manner

To investigate the role of p130Cas in ADM, we used a physiological cell culture model of ADM, consisting of the *in vitro* transdifferentiation of acinar explants embedded in collagen (Paoli & Carrer, 2020). In this experimental setting, $Kras^{G12D}$ expression or EGFR stimulation induces the formation of ductal structures from isolated acini (Figures A and B). In isolated pancreatic acini of Pdx^{Cre}; $Kras^{G12D}$, EGF treatment induced p130Cas phosphorylation in a dose-dependent manner (Figures 3C and D). After 5 days, acini treated with EGF or isolated from $Kras^{G12D}$ mice transdifferentiated and showed increased p130Cas expression and phosphorylation (Figures 3E, F, and G) compared with control acini. Furthermore, ectopic p130Cas expression increased the formation of ductal structures from $Kras^{G12D}$ acini, while short hairpin RNA-mediated p130Cas down-modulation had the opposite effect (Figures 3H and I). These data indicate that p130Cas expression levels are critical to mediate Kras-induced acinar metaplasia in a cell-autonomous manner.

Figure 3

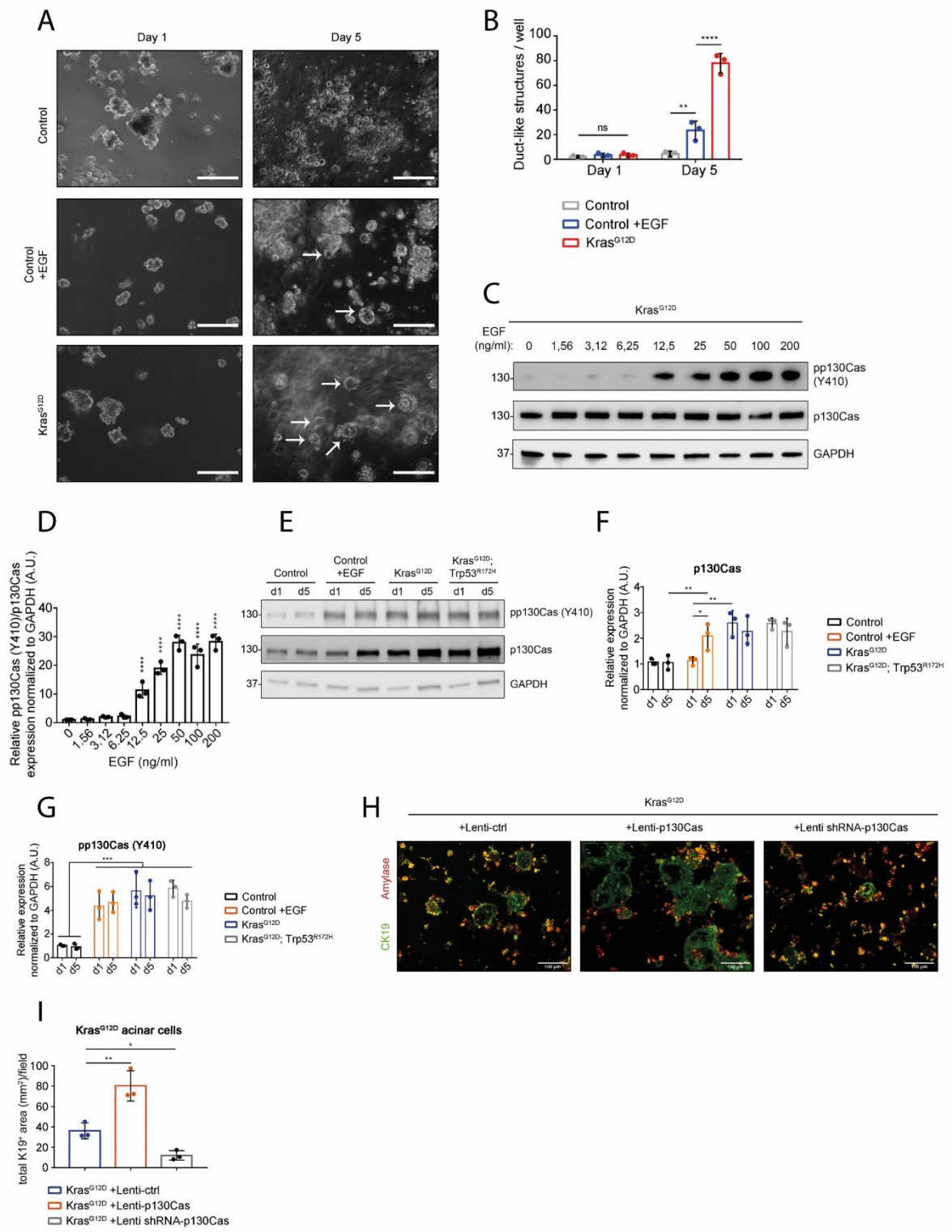

Figure 3. Cell-autonomous p130Cas expression is critical for ADM. (A, B) Formation of duct-like structures from primary acinar cells that were isolated from murine pancreata, seeded in 3D culture in collagen, and transdifferentiation was induced with EGF as indicated. (C, D) Primary acinar cultures were subjected to Western

blot to evaluate p130Cas phosphorylation (pp130Cas Y410) in response to increasing EGF concentration, as indicated. (E, F, G) Primary acinar cultures were subjected to Western blot to evaluate p130Cas phosphorylation (pp130Cas Y410) and expression, as indicated. The data reported are representative of at least 3 independent experiments. ∗∗P<0.01. (H, I) Primary acinar cells were transduced with lentiviral particles harboring ctrl, p130Cas, or short hairpin RNA against p130Cas and seeded as 3D culture. Immunofluorescent staining revealed amylase-positive acinar cells (red) or CK19-positive ductal structures (ADM) (green). The area stained by CK19 was quantified to score ADM formation. Statistical analyses were performed with a 2-way analysis of variance. Data are presented as mean ± SD.

p130Cas permits Kras-induced ADM formation by promoting PI3K-AKT signaling

It is known that EGF increases the number of ductal structures from $Kras^{G12D}$ explanted acini (Paoli & Carrer, 2020). Therefore, we tested the extent of EGF-induced ADM in the presence or absence of p130Cas. Remarkably, EGF stimulation failed to sensitize $Kras^{G12D}$; $p130Cas^{KO}$ acini to metaplastic transformation (Figures 4*A* and B). These data indicate that loss of p130Cas blocks EGFR signaling to ADM in the presence of a hyperactive $Kras^{G12D}$. Downstream of EGFR, p130Cas acts as a point of convergence between integrin and growth factor signaling; hence, its deletion could influence various signaling pathways (Cabodi, del Pilar Camacho-Leal, et al., 2010; Defilippi et al., 2006). To investigate which pathways were most affected by p130Cas during ADM, we analyzed the 3D culture of primary acini isolated from $Kras^{G12D}$ and $Kras^{G12D}$; $p130Cas^{KO}$ mice by Western blot. We observed a moderate reduction of Myc protein in $p130Cas^{KO}$ acini, but we did not detect any difference in β-catenin activation or FAK phosphorylation (Figures 4C and D). One of the most critical signaling events during ADM is the activation of the PI3K/AKT pathway (Baer et al., 2014; Carrer et al., 2019; Eser et al., 2013). In agreement, $Kras^{G12D}$ acini lacking p130Cas exhibited a reduction in AKT phosphorylation both in basal condition and in the presence of EGF, with less evident effects on MEK1/2 and ERK1/2 phosphorylation (Figures 4E, F, and G). This was not due to abnormal EGFR activation, as in the absence of p130Cas, EGF treatment efficiently

promoted an increase in EGFR, AKT, MEK1/2, and ERK1/2 phosphorylation in acinar explants (Figures 4E, F, and G).

In line with the view that p130Cas specifically amplifies targeted EGFR signaling, it has already been demonstrated that phosphorylated p130Cas directly binds to p85α PI3K-regulatory subunit, promoting PI3K activation (Li et al., 2000; Riggins et al., 2003). We thus hypothesized that p130Cas might directly regulate PI3K activity in pancreatic acinar cells. To this end, we first tested the p130Cas-p85α association in isolated $Kras^{G12D}$ acini. In basal conditions, p85α was barely detectable in p130Cas immunoprecipitates, but p85α–p130Cas interaction increased after 10 minutes of EGF stimulation (Figure 4H). Moreover, we observed that p85α efficiently co-immunoprecipitated with tyrosine-phosphorylated p130Cas on EGF stimulation (Figure 4H). To confirm that p130Cas directly contributes to PI3K activation, we measured PI(3,4,5)P3 levels in $Kras^{G12D}$ acini. We found that the loss of p130Cas significantly reduces the production of this lipid second messenger in basal conditions and, more strikingly, in the presence of EGF (Figure 4I). This result showed that cell-autonomous p130Cas expression supports PI3K-AKT signaling and permits Kras-induced ADM formation.

Figure 4

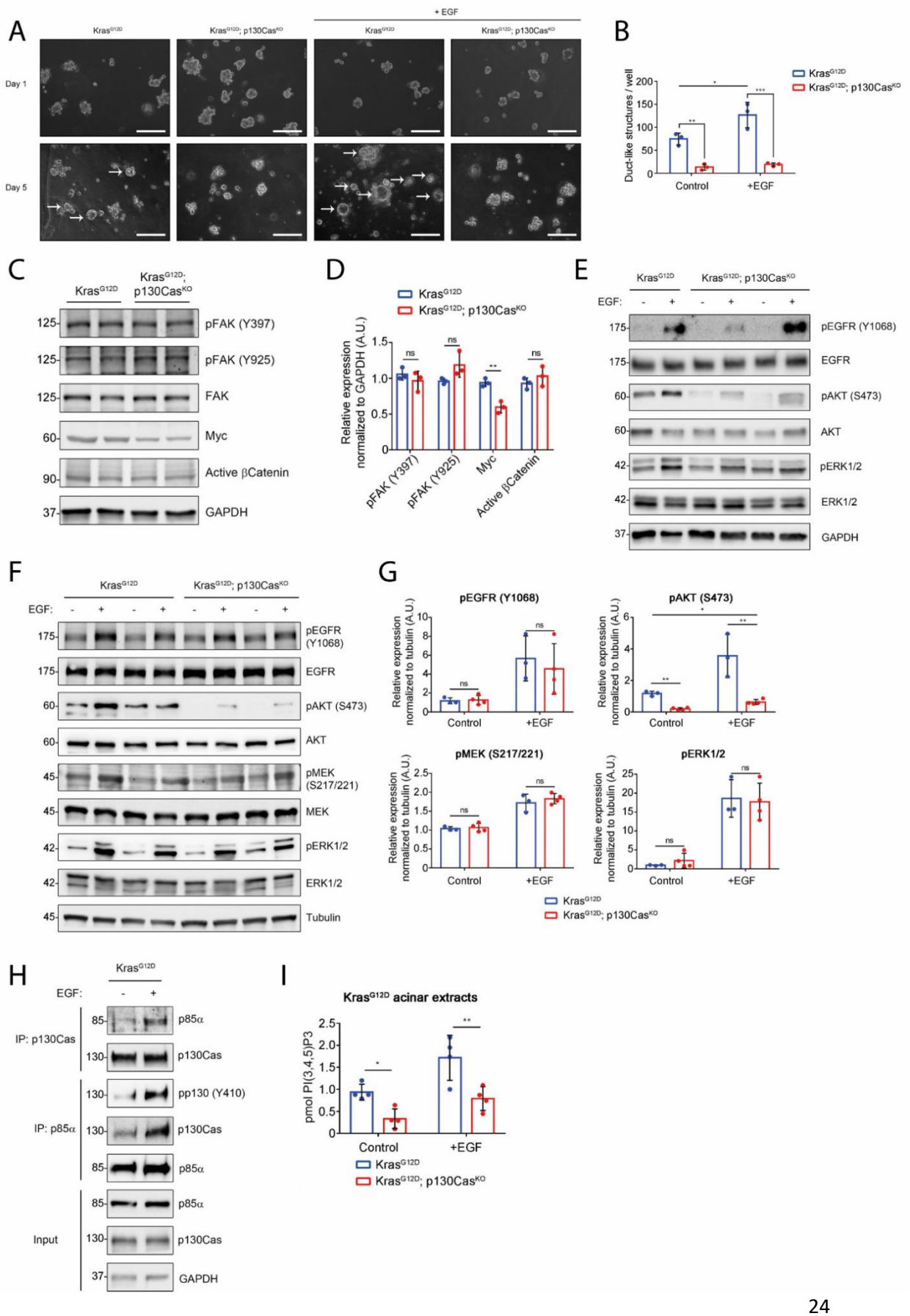
A
+ EGF
Day 1
Day 5
B
Duct-like structures / well
Control
+EGF
C
pFAK (Y397)
pFAK (Y925)
FAK
Myc
Active βCatenin
GAPDH
D
Relative expression normalized to GAPDH (A.U.)
E
EGF:
pEGFR (Y1068)
EGFR
pAKT (S473)
AKT
pERK1/2
ERK1/2
F
pMEK (S217/221)
MEK
Tubulin
G
pEGFR (Y1068)
pAKT (S473)
pMEK (S217/221)
pERK1/2
Relative expression normalized to tubulin (A.U.)
H
IP: p130Cas
IP: p85α
Input
p85α
p130Cas
pp130 (Y410)
I
Kras^G12D acinar extracts
pmol PI(3,4,5)P3

Figure 4. p130Cas permits Kras-induced ADM formation by promoting PI3K-AKT signaling. (A, B) Primary acinar cells were isolated from KrasG12D and KrasG12D; p130CasKO murine pancreata, seeded in 3D culture in collagen and followed for spontaneous or EGF-induced transdifferentiation. Ducts (arrows) formed were photographed and counted. Scale bar: 100 μm. On the side, quantification of the duct-like structures. (C, D) Western blot analysis of primary acinar cells isolated from KrasG12D and KrasG12D; p130CasKO murine pancreata. The data reported are representative of at least 3 independent experiments. (E, F) Western blot (WB) of primary acinar cells isolated from murine pancreata and treated with phosphate-buffered saline (PBS) or EGF for 10 minutes, as indicated. (G) Quantification of (F). (H) Primary acinar cells isolated from murine pancreata were treated with PBS or EGF for 10 minutes and subjected to immunoprecipitation with anti-p130Cas and anti-p85α antibodies. p130Cas/p85α interaction was revealed by WB with anti–phospho-p130Cas (pp130Cas Y410), anti-p130Cas, or anti-p85α antibodies as indicated. (I) Primary acinar cells isolated from murine pancreata were treated with PBS or EGF for 10 minutes and subjected to lipid extraction and PI(3,4,5)P3 enzyme-linked immunosorbent assay (ELISA).

3.3. Materials and Methods

Mice. The LSL-Kras^{G12D} and LSL-p53^{R172H} knock-in (from D. Tuveson, Mouse Models of Human Cancers Consortium repository, National Cancer Institute-Frederick), Pdx1Cre (from D.A. Melton, Harvard University, Cambridge, MA) and p130Cas$^{fl/fl}$ (from S. Cabodi, University of Torino) strains were interbred on a mixed background (SV129/C57Bl6) to obtain compound mutant PdxCre; Kras^{G12D} (named Kras^{G12D}), PdxCre; Kras^{G12D}; Trp53^{R172H} (named Kras^{G12D}; p53^{R172H}), PdxCre; Kras^{G12D}; p130CasKO (named Kras^{G12D}; p130CasKO). Pdx1Cre mice of the same age were used as controls. All procedures and animal housing conformed to the regulatory standards. The ethical committee approved them according to the Guide for the Care and Use of Laboratory Animals published by the U.S. National Institutes of Health and approved by the Italian Health Minister (authorization no. 64-2016PR).

Preparation of Pancreatic Epithelial Explants Culture. The procedure to isolate primary pancreatic acinar cells was described in detail previously (Means et al., 2005; Paoli & Carrer, 2020). In brief, the pancreas was removed, washed twice with ice-cold Hank's balanced salt solution (HBSS) media, minced into 1–5 mm pieces, and digested with collagenase I (37 °C, shaker). Collagen digestion was stopped by adding an equal volume of ice-cold HBSS media containing 5% fetal bovine serum (FBS). The digested pancreatic pieces were washed twice with HBSS media containing 5% FBS and pipetted through 500 mm and 105 mm meshes. The supernatant of the cell suspension containing acinar cells was added dropwise to 20 ml HBSS containing 30% FBS. Acinar cells were then pelleted (1,000 rpm, 2 min at 4°C), re-suspended in 10 ml RPMI complete media (1% FBS, 0.1 mg/ml trypsin inhibitor, 1 mg/ml dexamethasone), and plated into low-adhesion dishes for standard culture. For the 3D explant culture, cell culture plates were coated with collagen I. Isolated primary pancreatic acinar cells were added as a mixture with collagen I/medium media on the top of this layer. Further, complete media was

added on top of the cell/gel mixture, replaced the following day, and then every other day.

PI(3,4,5)P3 Quantification. PI(3,4,5)P3 levels were measured by ELISA kit (Echelon Bioscience, K2500) following manufacturer protocol.

***Protein Analysis*.** Cells were homogenized in lysis buffer (120 mM NaCl, 50 mM Tris-HCl pH = 8, 1% Triton X-100) supplemented with 25x protease inhibitor cocktail (Roche), 50 mM sodium fluoride and 1 mM sodium orthovanadate. Lysates were cleared by centrifugation at 13,000 rpm for 15 min at 4°C. The Bradford method determined protein concentration, and supernatants were analyzed for immunoblotting or immunoprecipitation (IP) with the indicated antibodies. Membranes probed with the indicated antibodies were then incubated with HRP-conjugated secondary antibodies (anti-mouse used 1:10000, anti-rabbit 1:5000, Sigma) and developed with enhanced chemiluminescence (ECL, Biorad). For IP assays, cells were lysed in IP lysis buffer (150 mM NaCl, 50 mM Tris [pH 7.5], 1% Igepal CA-630, 0.5% deoxycholate), and 1 mg of pre-cleared extracts were incubated with 1 µg of the indicated antibody at 4°C on a rotating rack overnight. Then 15 µl of protein G-Dynabeads (ThermoFisher) were added for 2 hours. Samples were collected by centrifugation (13,000 rpm 1 min) and washed six times with IP lysis buffer. Bound protein complexes were then eluted by adding 30 µl Laemmli sample buffer.

Antibodies and Reagents. Cell treatments: recombinant murine EGF (PeproTech; #215-09; working concentration: 50 ng/ml unless otherwise specified), recombinant human TGFα (PeproTech; #100-16A; 50 ng/ml); LY294002 (Sigma Aldrich; #440202; 10 µM). Mouse monoclonal antibodies to human/murine p130Cas were produced in our department. Additional p130Cas antibodies were purchased from BD Transduction Laboratory (Material number 610272) and Cell Signaling Technology (clone E1L9H, #13846). Antibodies against ERK1/2 (4696),

P-ERK1/2 (4370), AKT (2920), P-AKT (9271 and 9277), pMEK1/2 (9121), MEK1/2 (4694), Myc (5605), Active β-Catenin (8814), Tubulin, GAPDH (2118), were from Cell Signaling Technology. Antibodies against Amylase (A8273) and CK19 (MABT913) were from Sigma Aldrich.

Histology and Immunohistochemistry. Mice tissues were fixed with 10% buffered formalin solution overnight and embedded into paraffin by the institutional pathology core laboratory. Sections cut from the paraffin block were stained with hematoxylin/eosin, following standard protocols. For immunolabeling, unstained 5-mm sections were cut from paraffin blocks. The slides were deparaffinized by routine techniques followed by incubation in 1X sodium citrate antigen retrieval buffer (ThermoFisher) before steaming for 20 minutes in a pressure cooker. Slides were cooled for 2 hours, blocked, and incubated overnight with primary antibodies. Immunolabeling was detected using Novolink Polymer Detection System (Leica Biosystems), and sections were counterstained with hematoxylin. For immunolabeling, the staining intensity was scored and assigned based on this scale: 0 (absent), 1 (low positive signal), 2 (moderately strong positive signal), and 3 (strong positive signal).

Statistical Analysis. Prism software (GraphPad) was used for statistical analysis. Significance was calculated with a Student t-test and one- or two-way analysis of variance tests (ANOVA) followed by Bonferroni's post hoc analysis or Mantel-Cox log-rank test where appropriate. Values are reported as mean ± SD.

3.4. Discussion

PDAC progression is thought to occur gradually. Early detection is difficult, though, and late diagnosis is a major contributor to the high fatality rate. A better understanding of the early steps that lead to PDAC initiation is crucial. It is critical to have a better knowledge of the preliminary processes leading to PDAC initiation. ADM is now recognized as a key precursor to PanIN lesions and the development of pancreatic cancer, although our knowledge of the underlying mechanisms is still lacking (Bailey et al., 2014; Storz, 2017; Storz & Crawford, 2020). In this work, we demonstrated the critical function of p130Cas expression during acinar metaplasia that occurs through the regulation of the PI3K–AKT pathway.

According to the data we collected from $Kras^{G12D}$ mice, the metaplastic transition of acinar cells toward ductal intermediates coincides with the rise in p130Cas levels. However, p130Cas up-regulation during ADM was not restricted to $Kras^{G12D}$ cells; Indeed, it also occurred in normal acini treated with EGF. The metaplastic transition primes acinar cells to $Kras^{G12D}$ oncogenic transformation that promotes the formation of pre-invasive lesions (Li et al., 2021). We found that raising p130Cas levels also increased $Kras^{G12D}$-induced ADM, demonstrating the significance of p130Cas in the first stages of PDAC development.

The expression of mutant $Kras^{G12D}$ in the murine pancreas is sufficient to initiate ADM, keeping metaplastic cells in a duct-like state (Hingorani et al., 2003). However, this has a moderate penetrance and a prolonged latency, which explains why additional genetic defects, persistent inflammation, or an increase in growth factor signaling are needed for effective ADM induction and transformation of pancreatic acinar cells (Guerra et al., 2007; Storz, 2017; Storz & Crawford, 2020). Previous studies showed that both EGFR and Kras signaling converge to upregulate PI3K activity and drive acinar metaplasia (Ardito et al., 2012). Notably, whereas resident mutant Kras partially activates the PI3K-AKT

pathway, EGFR-mediated signaling is still required to boost this activation (Blasco et al., 2019).

Mechanistically, the activation of PI3K signaling by $Kras^{G12D}$ is mediated by its direct binding to the p110 catalytic subunit (Blasco et al., 2019; Castellano & Downward, 2011). To fully activate the PI3K-AKT pathway, however, the interaction of the p85 regulatory subunit with phosphotyrosines is still necessary (Jimenez et al., 2002). In v-Crk (Avian Sarcoma Virus CT10 Oncogene Homolog)-transformed cells, phosphorylated-p130Cas interacts with p85 to enhance PI3K activity (Li et al., 2000; Riggins et al., 2003). In line with this result, we showed that phosphorylated-p130Cas binds to p85 in our cell-based model, enabling complete PI3K-AKT activation by oncogenic Kras. As a result, we discovered that PI3K activity downstream of EGFR and $Kras^{G12D}$ was reduced because of p130Cas loss. Inactivation of p110α is sufficient to block ADM induced by inflammation and oncogenic Kras, thereby suppressing pancreatic cancer initiation(Baer et al., 2014). In agreement, the same phenotypes were recapitulated by p130Cas deletion in mouse models. Our data demonstrated that loss of p130Cas was sufficient to prevent $Kras^{G12D}$-induced ADM, resulting in complete protection from a single $Kras^{G12D}$ mutation.

In addition to the PI3K-AKT axis, p130Cas may also regulate the DOCK1-RAC1-β-catenin axis, Myc down-regulation, or activation of FAK and integrin signaling during Kras-dependent carcinogenesis and progression (Cabodi, del Pilar Camacho-Leal, et al., 2010; Katoh, 2020; Waters et al., 2021). Our study confirmed that p130Cas deletion downregulates Myc expression, although this down-regulation was moderate, and β-catenin activation was unaltered. Although seemingly contrasting with previous reports (Waters et al., 2021), different experimental settings may account for the apparent discrepancy. For instance, our 3D cultured primary acini, which were isolated before Kras acinar metaplasia, did not proliferate at the same rate as 2D-grown, fully transformed cancer cell lines. In addition, FAK activation was unexpectedly normal in our 3D-

grown p130Cas-deficient acinar cells. Although p130Cas is a crucial component of the integrin signaling cascade and a sensitive mechanosensor, it is possible that our cell culture conditions modified adhesion-mediated signaling. Although other adaptor proteins, for example, Paxillin, might have replaced p130Cas in 3D cultures, further studies are needed to fully clarify why the loss of p130Cas mainly impacts the PI3K pathway and no other signaling cascades.

4. p140Cap modulates the mevalonate pathway decreasing cell migration of breast cancer cells and controlling lipid-raft signaling

4.1. Introduction

Cholesterol is a crucial metabolite of mammalian cells; it controls the structural integrity and fluidity of the plasma membrane and is implicated in regulating signaling pathways involved in cell proliferation, immunity, and inflammation (Luo et al., 2020). Cholesterol is synthesized through a series of more than 20 reactions collectively called the mevalonate (MVA) pathway. Besides being the biosynthetic route for cholesterol, the MVA pathway generates non-sterol isoprenoids, including isopentenyl pyrophosphate (IPP), farnesyl pyrophosphate (FPP), and geranylgeranyl pyrophosphate (GGPP) (Faulkner & Jo, 2022). FPP and GGPP are used for the prenylation of the Ras, Rho, and Rab superfamily of GTPases, leading to their membrane localization and activation. Moreover, the MVA pathway generates the isoprene subunits for the biosynthesis of ubiquinone (UQ). This redox-active lipid molecule acts as a cofactor for numerous enzymes, including those of the mitochondrial electron transport chain (Stefely & Pagliarini, 2017).

The flux through the MVA pathway is tuned by feedback mechanisms that regulate the level and the activity of critical enzymes to ensure the generation of appropriate levels of all the MVA metabolic products and intermediates. The principal enzyme subjected to feedback control is 3-Hydroxy-3-methyl glutaryl coenzyme A (HMG CoA) reductase (HMGCR). This enzyme catalyzes the rate-limiting step of the MVA pathway, the reduction of HMG-CoA to mevalonate. HMGCR receives stringent feedback control by downstream metabolites through transcriptional and post-translational mechanisms (Faulkner & Jo, 2022). The HMGCR gene's transcription is controlled by sterol regulatory element binding proteins (SREBPs). Specifically, the master regulator of HMGCR and other MVA

pathway genes is the SREBP2 isoform. In a condition of cholesterol sufficiency, SREBP2 resides in the endoplasmic reticulum (ER) membrane in an inactive form (Horton et al., 2002). Upon cholesterol depletion, specifically when intracellular cholesterol levels reach 5mol% of total ER lipids, SREBP2 interacts with the SREBP-cleavage activating protein (SCAP), which binds to COPII-coated vesicles that transport the SCAP/SREBP complex from the ER to the Golgi. Then, SREBP2 is sequentially cleaved by site 1 protease (S1P) and site 2 protease (S2P), releasing the active SREBP2 N-terminal domain that enters the nucleus and binds to the sterol-responsive element (SRE) in the promoters of HMGCR and other genes involved in cholesterol homeostasis, including the low-density lipoprotein receptor (LDLR), enhancing the gene transcription (Xue et al., 2020). In contrast, when intracellular cholesterol rises, the SREBP/SCAP complex associates with the insulin-inducible gene proteins (INSIGs), which retain the SCAP/SREBP complex in the ER. Thus, SREBP is not cleaved, and the transcription of genes involved in cholesterol synthesis and uptake decreases.

HMGCR levels are controlled by sterols (lanosterol, DHL, and oxysterols) and the nonsterol isoprenoid GGPP through post-transcriptional mechanisms (Faulkner & Jo, 2022). Excess of these metabolites promotes the extensive ubiquitination of HMGCR and the subsequent ER-associated degradation (ERAD) of HMGCR (Guerra et al., 2021). Another level of regulation is achieved by the reversible phosphorylation of Serine 872 by AMP-activated protein kinase (AMPK), which decreases the HMGCR activity (Omkumar & Rodwell, 1994).

Alterations in cholesterol metabolism are a metabolic hallmark in several cancers, and fast-proliferating cancer cells require high cholesterol levels for membrane biogenesis and other functional needs (Centonze, Natalini, Piccolantonio, et al., 2022; Chimento et al., 2018; Mullen et al., 2016). High cholesterol levels determined by enhanced biosynthesis and uptake and reduced cholesterol efflux have been reported to accelerate malignant cell growth, cell migration, metastatization, cancer stem cell features, and angiogenesis (Göbel et al., 2022).

Furthermore, these metabolic features are associated with shorter survival in pre-clinical models of breast cancer and when considering patient studies (Alikhani et al., 2013; Baek et al., 2017; Brindisi et al., 2020; dos Santos et al., 2014; Gallagher et al., 2017; Pelton et al., 2014). However, different studies reported no or even an inverse association between these cholesterol signatures and patient outcomes, indicating that the role of cholesterol metabolism in breast cancer patients is still controversial and needs to be deeply dissected (Touvier et al., 2015; Wei et al., 2021). Therefore, it seems critical to better elucidate the effect of cholesterol and its derivatives in breast cancer cell biology, considering the multifactorial nature and the heterogeneity of cancer.

Cholesterol plays a crucial role in the control of membrane fluidity. This physical parameter determines the rate of movement of molecules in the membrane and influences several aspects of cancer cell behavior, including adhesion, cell motility, and epithelial-to-mesenchymal transition (EMT). Recent studies show that high cholesterol levels in the plasma membranes determine reduced fluidity, which negatively regulates the metastatic potential of breast cancer cells (Zeisig et al., 2007; Zhao et al., 2016).

Here, we describe p140Cap as a crucial regulator of cholesterol metabolism in BC cells. We demonstrate that p140Cap promotes the metabolic flux through the MVA pathway by inducing HMGCR transcription via SREBP2 activation and reducing HMGCR ubiquitin-dependent degradation. Moreover, p140Cap favors cholesterol accumulation in the plasma membrane, leading to a reduced membrane fluidity that negatively controls cell migration. Finally, p140Cap localizes to lipid rafts and negatively regulates Rac1 activity.

4.2. Results

p140Cap increases the metabolic flux through the MVA pathway

To assess whether p140Cap can contribute to the metabolic landscape in BC cells, we took advantage of a previously described gene expression dataset obtained in p140Cap-overexpressing MDA-MB-231 (Sharma, Repetto et al. 2013). We performed a Gene Ontology (GO) analysis revealing an enrichment in genes related to the "sterol metabolic process" (GO:0016125) and "cholesterol metabolic process" (GO:0008203) in p140Cap cells (Figure 5A, Table 1). To investigate the role of p140Cap in the cholesterol metabolism of BC cells, we modulated p140Cap expression by gain of function or silencing approaches in triple-negative and Her2-positive human BC cell lines MDA-MB-231 and SKBR3, respectively (Grasso, Chapelle et al. 2017). Moreover, we also used the Her2-positive TUBO cell line, established from the BALB/c-MMTV-NeuT mouse model (Rovero et al., 2000) (Figure 5B). Therefore, we assessed the metabolic flux through the cholesterol biosynthetic pathway, also known as the MVA pathway (Figure 5C), by measuring the synthesis of metabolites cholesterol, GGPP, and UQ. MDA-MB-231, SKBR3, and TUBO p140Cap cells had a significantly increased synthesis of these molecules compared to mock cells (Figures 5D, E, and F). Notably, silencing endogenous p140Cap protein in SKBR3 cells reduces the production of these three metabolites, suggesting that p140Cap generally affects the MVA pathway in different BC cellular models. Interestingly, transient expression of p140Cap in HEK293T cells was sufficient to increase cholesterol, GGPP, and UQ synthesis (Figures 5B, D, E, and F), indicating that p140Cap controls the MVA pathway even upon a short time expression and in a non-BC cell line. To assess whether the p140Cap-dependent increased synthesis of the MVA pathway metabolites was still sensitive to well-known MVA pathway drugs, we treated SKBR3 cells with the HMGCR inhibitor simvastatin (SIM) (Liao and Laufs 2005), the FPP synthase inhibitor zoledronic acid (ZA) (Roelofs, Thompson et al. 2006) and the squalene synthase inhibitor squalestatin (SQ) (Bergstrom, Dufresne et al.

1995). Cholesterol, GGPP, and UQ synthesis were downmodulated in mock and p140Cap cells similarly, according to the inhibited branch of the MVA pathway (Figure 5G, H, and I). These data show that the MVA pathway and the related targeted enzymes are still druggable and that p140Cap activity occurs upstream of the HMGCR catalytic reaction.

Figure 5

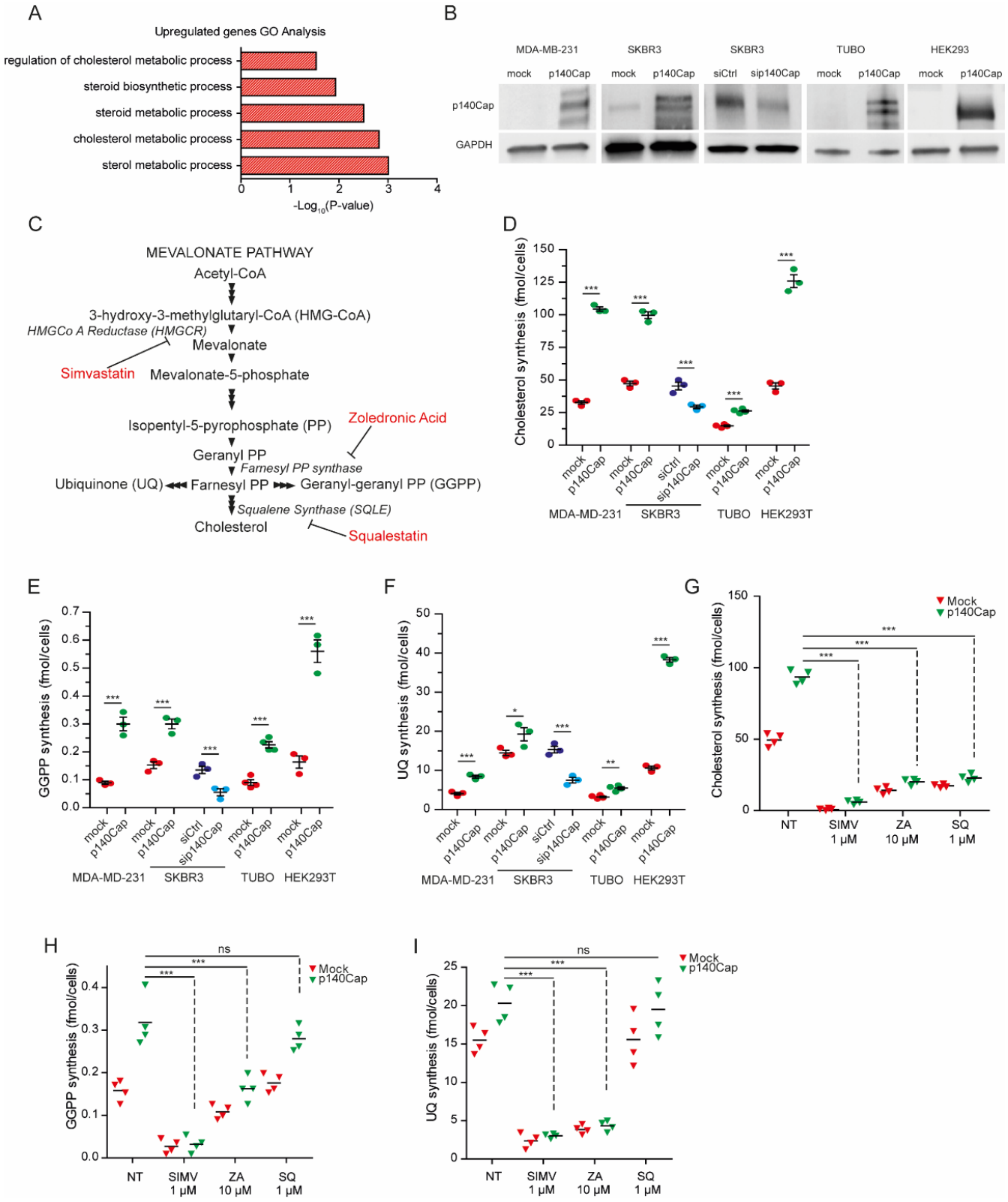

Figure 5. p140Cap increases the metabolic flux through the MVA pathway. (A) List of Gene Ontology terms related to cholesterol and lipid metabolism that are enriched in a dataset of up-regulated genes in MDA-MB-231 p140Cap cells. (B) Western

Blotting analysis of p140Cap expression in cell lines. GAPDH is used as a loading control. (C) Schematic representation of the MVA pathway with the main intermediates, enzymes, and inhibitors. (D) The *de novo* synthesis of cholesterol, (E) geranylgeranyl diphosphate (GGPP), and (F) ubiquinone (UQ) was measured by incubating with 1 μCi [^{3}H] acetate for 24 h, recovering the lipids, and measuring the radioactivity by liquid scintillation. Unpaired t-test (*P<0.01; **P<0.001; ***P<0.0001). Error bar: SEM. (G,H,I) Cholesterol, GGPP, and UQ synthesis in SKBR3 cells treated with the indicated concentration of the MVA pathway inhibitors Simvastatin (SIMV), Zoledronic Acid (ZA), and Squalestatin (SQ). ANOVA test and Bonferroni post-test (***P<0.0001), Error bar: SEM.

p140Cap controls HMGCR levels and activity through transcription and post-translational mechanisms

Considering that HMGCR is the rate-limiting enzyme of the MVA pathway, we evaluated its activity by measuring the amount of [14C] mevalonolactone generated upon incubation with the radiolabelled isoform of the HMGCR substrate HMG-CoA. In line with the observed enhanced synthesis of the end-products of the MVA pathway, we detected increased enzymatic activity of HMGCR by 50% in MDA-MB-231, SKBR3, TUBO, and HEK293T p140Cap cells compared to their mock counterparts (Figure 6A). On the other hand, p140Cap silencing in SKBR3 cells resulted in a 50% reduction of HMGCR activity (Figure 6A). The analysis of in vivo tumors, obtained by orthotopic injection of TUBO mock or TUBO p140Cap in Balb-c mice, showed the up-regulation of the HMGCR in p140Cap tumors compared to mock tumors of the same volume (approximately 500 mm3) (Figure 6B), indicating that the p140Cap-dependent tuning of the MVA pathway is maintained during tumor growth. The HMGCR enzymatic activity can be negatively controlled through phosphorylation at Ser872 by the AMP-activated protein kinase (AMPK) (Clarke & Hardie, 1990). Phosphoserine HMGCR levels were not affected in SKBR3 p140Cap cells compared to mock cells and even undetectable in MDA-MB-231 cells (Figure 6C), suggesting that AMPK-mediated phosphorylation is not a major mechanism for regulating HMGCR in p140Cap cells. (Figure 6C). We detected increased HMGCR protein in MDA-MB-231, SKBR3, and HEK293T p140Cap cells (Figure 6C). Therefore, we assessed the mRNA level

of HMGCR and other MVA pathway genes through quantitative real-time PCR, and we observed in SKBR3 p140Cap cells a statistically significant increase in HMGCR mRNA levels, and to a lesser extent, of SQLE and LSS genes, compared to mock cells (Figure 6D). HMGCR expression is tightly controlled at the transcriptional level according to the intracellular cholesterol content through the transcription factor SREBP2 (Burg & Espenshade, 2011). Therefore, we speculated that p140Cap could favor SREBP2 transcriptional activity. To evaluate this hypothesis, we measured the amount of cleaved SREBP2 cells by Western Blotting. p140Cap expression did not induce any differential activation of SREBP2 in terms of the amount of cleaved SREBP2 in HEK293T or MDA-MB-231 cells, growth in normal or in lipoprotein-depleted media (LD), a condition that boosts SREBP2 maturation (Figure 6E) We further investigated the activity of SREBP2 by using a reporter system in which the luciferase gene is under an SRE-containing promoter (Bertolio et al., 2019). Specifically, we transiently transfected HEK293T cells with plasmids encoding p140Cap, or an empty vector, together with the luciferase reporter plasmid harboring a wild-type (SREwt) or a mutated form (SREmut) of the SRE sequence. 24 h after transfection, we detected a significant increase in luminescence signal in p140Cap versus control cells, indicating that p140Cap promotes the transcriptional activity of SREBP2 (Figure 6F). The binding of SREBP2 to the SRE was specific since the reporter plasmid with the SREmut sequence did not induce any luminescence signal (Figure 6F).

Ubiquitination is also involved in the negative regulation of HMGCR, promoting its degradation through endoplasmic reticulum (ER)-associated proteasomal degradation to limit cholesterol production (Guerra et al., 2021). Moreover, the ubiquitination of HMGCR is the prerequisite for its proteasomal degradation, as suggested by the increased ubiquitinated levels of HMGCR in SKBR3 cells pre-treated with the proteasome inhibitor bortezomib (Figure 6G). Notably, we observed that MDA-MB-231 p140Cap, SKBR3 p140Cap, and HEK293T p140Cap cells consistently showed a pattern of reduced HMGCR ubiquitination (Figure 6H),

suggesting that p140Cap controls HMGCR protein stability. Overall, these data indicate that p140Cap upregulates the metabolic flux through the MVA pathway promoting the SREBP2-mediated transcription of HMGCR and maintaining high HMGCR protein levels by preventing its ubiquitination and proteasomal degradation. To assess the ability of p140Cap cells to detect changes in cholesterol levels and degrade HMGCR accordingly, we analyzed HMGCR ubiquitination status and protein levels upon cholesterol loading and depletion (Figure 6H). Cholesterol-loaded mock and p140Cap cells exhibited decreased HMGCR protein levels and increased ubiquitination, indicating that p140Cap cells can respond to enhanced cholesterol content. Conversely, when we treated cells with the cholesterol removal agent methyl-β-cyclodextrin (MβCD), mock cells were responsive, significantly decreasing cellular cholesterol and HMGCR ubiquitination while increasing HMGCR protein levels. Unfortunately, in p140Cap cells, cholesterol levels were not lowered by MβCD treatment, and therefore HMGCR protein and ubiquitination levels remain at the same level in untreated cells (Figure 6H, I). These data indicate that p140Cap cells have a pool of membrane cholesterol not fully available for MβCD action. Indeed, MβCD is a well-known chelator agent responsible for cholesterol depletion at the cell plasma membrane (Mahammad & Parmryd, 2015), and its reduced effect in p140Cap cells suggests a different membrane composition compared to that of mock cells. The increased cholesterol synthesis in p140Cap cells promoted by SREBP2 activity and HMGCR protein accumulation suggest a condition of low intracellular cholesterol. However, p140Cap cells exhibit total cholesterol levels like mock cells (Figure 6I). Similar results were also obtained in TUBO p140Cap tumors compared to mock tumors *in vivo* experiments (Figure 6J). Thus, these data suggest the presence of additional mechanisms that control the overall cellular cholesterol concentration. Finally, since both SREBP2 and HMGCR proteins are localized in the ER, by western blot analysis, we detected the presence of p140Cap in the microsomal fraction of BC cells, together with the

specific ER marker FAF2 (Figure 6K), suggesting that p140Cap could act in the same compartment where HMGCR and SREBP2 are present.

Figure 6

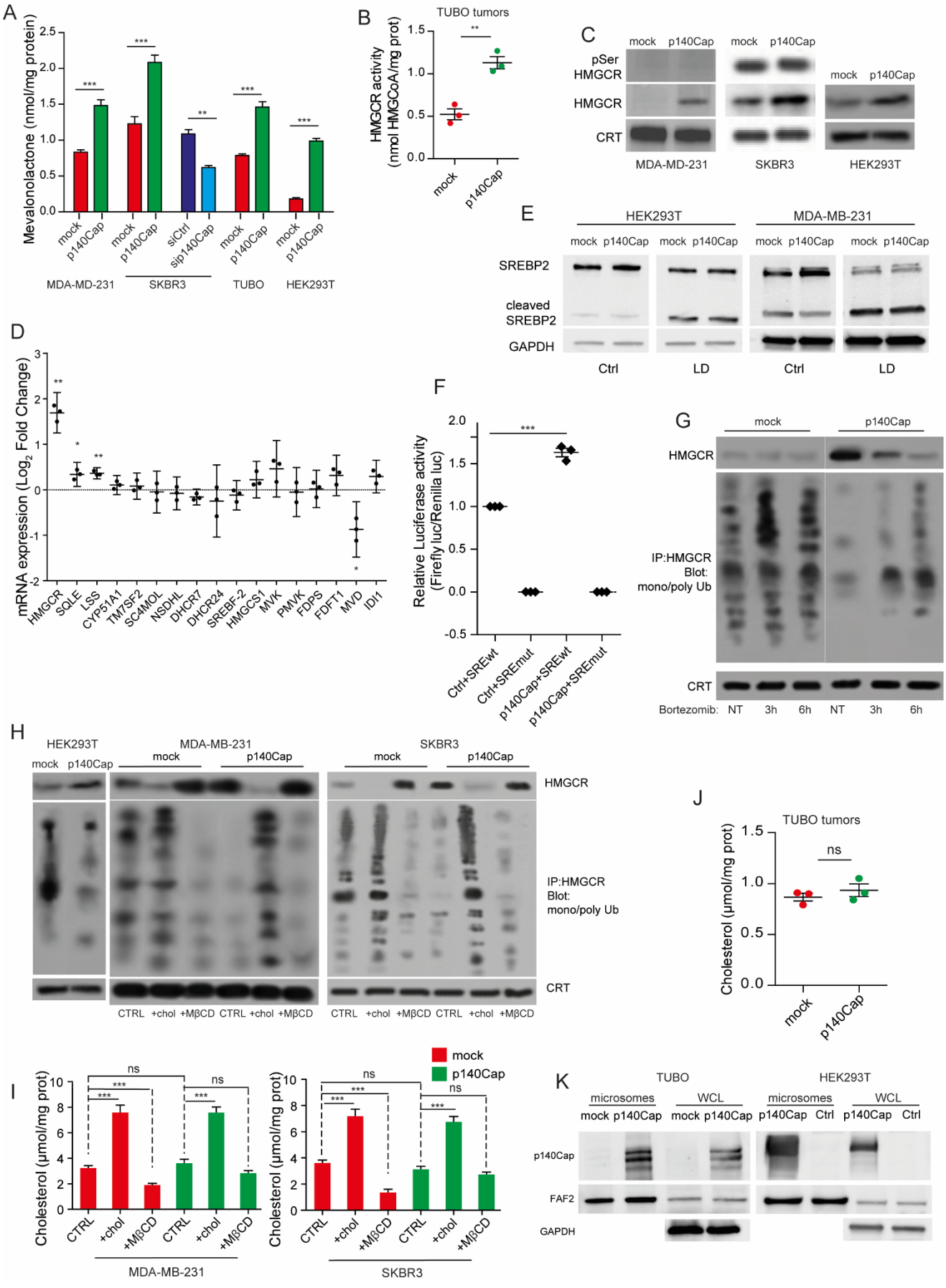
A
Mevalonolactone (nmol/mg protein)
mock p140Cap mock p140Cap siCtrl sip140Cap mock p140Cap mock p140Cap
MDA-MD-231 SKBR3 TUBO HEK293T
B
TUBO tumors
HMGCR activity (nmol HMGCoA/mg prot)
mock p140Cap
C
mock p140Cap mock p140Cap mock p140Cap
pSer HMGCR
HMGCR
CRT
MDA-MD-231 SKBR3 HEK293T
D
mRNA expression (Log2 Fold Change)
HMGCR SQLE LSS CYP51A1 TMTSF2 SC4MOL NSDHL DHCR7 DHCR24 SREBF-2 HMGCS1 MVK PMVK FDPS FDFT1 MVD IDI1
E
HEK293T MDA-MB-231
mock p140Cap mock p140Cap mock p140Cap mock p140Cap
SREBP2
cleaved SREBP2
GAPDH
Ctrl LD Ctrl LD
F
Relative Luciferase activity (Firefly luc/Renilla luc)
Ctrl+SREwt Ctrl+SREmut p140Cap+SREwt p140Cap+SREmut
G
mock p140Cap
HMGCR
IP:HMGCR Blot: mono/poly Ub
CRT
Bortezomib: NT 3h 6h NT 3h 6h
H
HEK293T MDA-MB-231 SKBR3
mock p140Cap mock p140Cap mock p140Cap
HMGCR
IP:HMGCR Blot: mono/poly Ub
CRT
CTRL +chol +MβCD CTRL +chol +MβCD CTRL +chol +MβCD
J
TUBO tumors
Cholesterol (µmol/mg prot)
ns
mock p140Cap
I
Cholesterol (µmol/mg prot)
mock
p140Cap
CTRL +chol +MβCD CTRL +chol +MβCD
MDA-MB-231 SKBR3
K
TUBO HEK293T
microsomes WCL microsomes WCL
mock p140Cap mock p140Cap p140Cap Ctrl p140Cap Ctrl
p140Cap
FAF2
GAPDH

Figure 6. p140Cap controls HMGCR through transcriptional and post-translational mechanisms. (A) For HMGCR activity, 60 nCi [^{14}C] HMG-CoA was added to microsomal extracts, and the labeled product Mevalonolactone was recovered and quantified by liquid scintillation. Unpaired t-test (**P<0.01;***P<0.001). Error bar: SEM. (B) HMGCR activity analyzed in tumors derived from mock and p140Cap TUBO cells orthotopically injected in Balb/c mice. (C) Immunoblot of immunoprecipitated HMGCR and pSer HMGCR. Calreticulin (CRT) was used as a loading control of microsomal extracts. (D) Quantification of mRNA levels of genes involved in the mevalonate pathway in SKBR3 p140Cap cells, relative to mock cells. (E) Immunoblot of SREBP2 in Ctrl and lipoprotein-depleted (LD) medium. (F) Analysis of SREBP2 activity by Dual Luciferase assay in HEK293T cells transiently transfected with the indicated vectors. (G) Immunoblot showing protein levels and ubiquitination of immunoprecipitated HMGCR following proteasomal inhibition with 500 nM Bortezomib for the indicated time in SKBR3 cells (H) Immunoblot showing protein levels and ubiquitination of immunoprecipitated HMGCR. When indicated, measurements were performed following cholesterol loading (+chol) and depletion (+MβCD). CRT was used as loading control. (I) Quantifications of Cholesterol in loading/depletion experiments. Cholesterol was measured using the Cholesterol Fluorimetric Assay kit and is expressed as µmol cholesterol/mg cell proteins. ANOVA test and Bonferroni post-test (***P<0.0001), Error bar: SEM. (J) Measurement of cholesterol levels in tumors in Balb/c mice derived from mock and p140Cap TUBO cells. Unpaired t-test. Error bar: SEM. (K) Immunoblot analysis of p140Cap in microsomal fractions and whole cell lysates of TUBO and HEK293T cell lines. The ER-resident FAF2 protein was used as a loading control.

p140Cap increases cholesterol efflux through ABC transporters

The data above show that the overall cholesterol content remains unchanged in p140Cap cells despite increased cholesterol synthesis by enhanced HMGCR mRNA, protein, and activity (Figure 6). Since the level of intracellular cholesterol results from the dynamic balance between synthesis, uptake, and export (Centonze, Natalini, Piccolantonio, et al., 2022; Luo et al., 2020), we reasoned that once synthesized, cholesterol could be rapidly effluxed from p140Cap cells to avoid the accumulation of potentially toxic excess of cholesterol. Therefore, we analyzed cholesterol efflux by measuring the levels of radiolabelled cholesterol released in the medium of MDA-MB-231, SKBR3, and HEK293 cells previously incubated with 1 µCi/ml [3H] cholesterol for 1 h, washed, and grown in a fresh medium for 24 h. p140Cap cells displayed at least a threefold increase in cholesterol efflux compared to mock cells (Figure 7A). Consistently, p140Cap silencing in SKBR3 cells leads to a 50% decrease in cholesterol efflux compared to

control cells (Figure 7A). In line with the increased efflux, p140Cap cells exhibited enhanced ATPase activity of the main transporters involved in cholesterol efflux, namely ATP-binding cassette A1 (ABCA1) and G1 (ABCG1) (Figure 7B). These data suggest that although p140Cap cells synthesize more cholesterol than mock cells, the overall cholesterol content remains unchanged, likely due to the enhanced ABCA1 and ABCG1-mediated cholesterol efflux. We next asked whether the increased cholesterol synthesis observed in p140Cap cells resulted from the enhanced cholesterol export or *vice versa*. To address this question, we compared cholesterol efflux between mock and p140Cap cells with similar levels of cholesterol synthesis. To this aim, we treated p140Cap cells with 1 µM simvastatin to partially inhibit HMGCR and reduce the synthesis of cholesterol, GGPP, and UQ to a level similar to mock cells (Figure 7C, D). Accordingly, upon simvastatin treatment of p140Cap cells, the HMGCR activity dropped in mock untreated cells (Figure 7E, F). In parallel with the lowered amount of synthesized cholesterol in simvastatin-treated MDA-MB-231 and SKBR3 p140Cap cells, cholesterol efflux was reduced to a level comparable to that of untreated mock cells (Figure 7G, H). These data suggest that the augmented cholesterol efflux observed in p140Cap cells could directly result from the increased MVA pathway flux to maintain an adequate cholesterol concentration inside the cells.

Figure 7

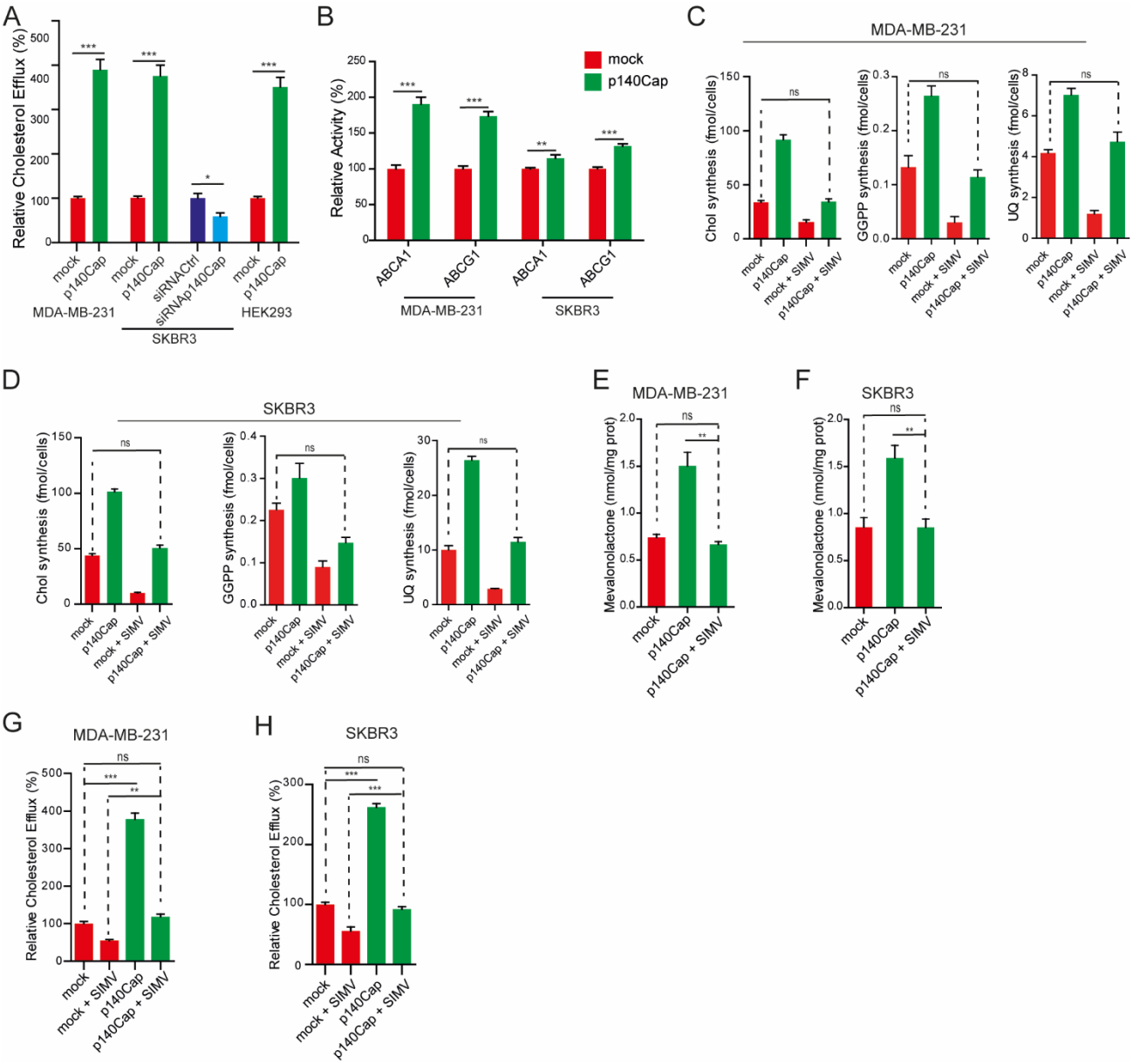

Figure 7. p140Cap increases cholesterol efflux through enhanced activity of ABCA1 and ABCG1. (A) For cholesterol efflux analysis cells were incubated with 1 µCi/ml with [3H] cholesterol, washed and let grow in a fresh medium for 24 h. Media was collected, cholesterol was extracted and quantified by liquid scintillation. The amount of [^{3}H] cholesterol exported from mock cells was considered 100%; Unpaired t-test (*P<0.05;***P<0.001).Error bar: SEM. (B) Evaluation of ABCA1/ABCG1 activity: ABCA1 and ABCG1 were immunoprecipitated from plasma membrane vesicles and the ATPase activity was measured by a spectrophotometric assay. The absorbance was converted into µmol hydrolyzed phosphate/min/mg proteins. ATPase activity was expressed as a percentage towards mock cells. (C-D) Cholesterol, GGPP, and UQ synthesis upon 1uM SIMV treatment for 48 h. (E-F) Relative HMGCR activity in cells treated with 1 uM SIMV for 48 h. (G-H) Cholesterol efflux measured upon 1uM SIM

treatment for 48 h. ANOVA test and Bonferroni post-test (**P<0.001; ***P<0.0001), Error bar: SEM.

p140Cap decreases membrane fluidity impairing BC cell migration ability

The ability of cancer cells to migrate and form metastasis can be affected by cholesterol levels in the plasma membrane (Zeisig et al., 2007; Zhao et al., 2016). Cholesterol is a crucial determinant of membrane fluidity - a physical property defined as the freedom of movement of a molecule within the cell membrane. Given the aberrant cholesterol synthesis and the previously described impairment in migration ability observed in p140Cap cells (Grasso et al., 2017), we hypothesize that by promoting cholesterol distribution to the plasma membrane and reducing membrane fluidity, p140Cap could impact cell migration. To assess this hypothesis, we evaluated the amount of free cholesterol in the plasma membrane. We observed a significantly increased level of plasma membrane cholesterol in MDA-MB-231, SKBR3, and TUBO cell lines expressing p140Cap (Figure 8A). Similar data were obtained in membranes derived from TUBO p140Cap tumors (Figure 8B). According to the increased membrane cholesterol in the plasma membrane, p140Cap cells also displayed decreased membrane fluidity compared to mock cells (Figure 8C). As expected, when we load cholesterol into the cells, we observe a reduction in membrane fluidity in all our samples. Notably, cholesterol-loaded mock cells displayed a membrane fluidity similar to that observed in uncharged p140Cap cells (Figure 8C). To further assess if the impaired migration ability observed in p140Cap cells may also depend on the reduced membrane fluidity, we performed a wound healing migration assay modulating membrane fluidity through cholesterol loading in MDA-MB-231 cells. Notably, at 48h upon scratch, we observed a complete wound closure by mock cells (Figure 8D, E, panels a-b) while, as expected, p140Cap cells migrate less, showing a 52% closure (Figure 8D, E, panels e-f). Cholesterol-loaded mock cells showed a percentage of wound closure similar to that observed in untreated p140Cap cells (Figure 8D, E, panels c-d). On the other hand,

cholesterol-loaded p140Cap cells migrate less than untreated cells, although the difference in wound closure was not statistically significant (Figure 8D, E, panels g-h). Overall, these data indicate that cells expressing p140Cap display increased membrane cholesterol and reduced membrane fluidity impairing cell migration in a cholesterol-dependent manner.

Figure 8

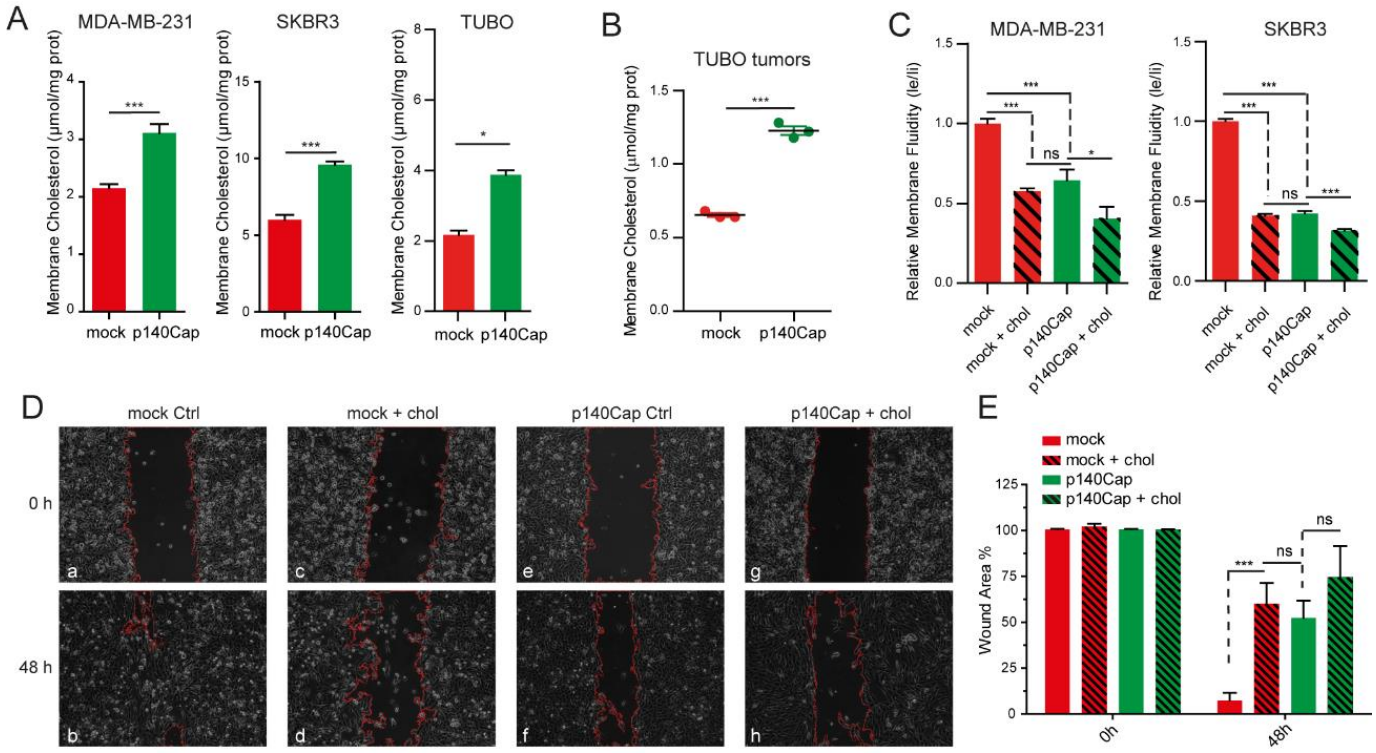

Figure 8. p140Cap decreases membrane fluidity impairing cell migration ability. (A) Membrane cholesterol quantification. Unpaired t-test (*P<0.01; ***P<0.0001, Error bar: SEM). (B) Cholesterol measurement of membranes derived from TUBO mock and p140Cap tumors. (C) Membrane fluidity was measured in cholesterol loading/depletion conditions using a membrane fluidity kit according to the manufacturer's protocol. ANOVA and Bonferroni post-test (*P<0.01; ***P<0.001; Error bar: SEM) (D) Representative images of Wound healing migration assays. $1x10^6$ MDA-MB-231 cells were seeded in each well and allowed to reach confluence as a monolayer. The monolayer was scratched across the center of the well and gently washed to remove the detached cells. Cells were cholesterol loaded and allowed to migrate for 48 h. (E) Quantification of the wound area. ANOVA and Bonferroni post-test (***P<0.001; Error bar: SEM).

p140Cap modulates Rac1 activity in lipid rafts of breast cancer cells

Cholesterol plays a crucial role in the formation of lipid rafts, which are small (10-200 nm), highly dynamic, sterol- and sphingolipid-enriched domains that act as organizing centers for the assembly of signaling molecules, regulating cellular signaling and biological processes, including cell migration (Lee et al., 2020; Vona et al., 2021). We investigated whether p140Cap could affect the organization of lipid rafts by analyzing the fluorescent signal of cholera toxin B (CTxB). This well-known lipid raft marker recognizes and binds glycolipid receptor ganglioside GM1 (Skočaj et al., 2013). Flow-cytometry analysis on CTxB-labelled cells revealed an increase in the mean intensity of CTXB fluorescence in MDA-MB-231 p140Cap and SKBR3 p140Cap cells compared to mock cells, indicating an increase in the lipid raft domain (Figure 9A, B). We have previously shown that p140Cap exhibits scaffolding functions at the plasma membrane and modulates protein localization at lipid rafts in neurons (Angelini et al., 2022; Chapelle et al., 2020). Therefore, we evaluated p140Cap lipid raft localization in MDA-MB-231 cells via Western Blotting analysis of isolated TritonX-100-insoluble membrane fractions obtained through a sucrose density gradient centrifugation (Rodgers & Rose, 1996). Fractions enriched in Flotillin-1 (fractions 4-5) contain lipid rafts, whereas ferritin receptor (CD71)-positive fractions (fractions 10-11) represent the non-lipid rafts compartment (Figure 9C). Results revealed that p140Cap is present in non-lipid raft fractions, as expected, but also in Flotillin-1-positive fractions, indicating that in BC cancer cells, p140Cap is a component of the lipid raft compartment and suggesting its putative ability to modulate signaling events related to lipid raft domains (Figure 9C). We have already shown that p140Cap curbs Rac1 activity by negatively regulating its GEF Tiam1 in Her2-amplified BC cell lines (Chapelle et al., 2020; Grasso et al., 2017) Accordingly, we assessed whether p140Cap could modulate Rac1 activity in the MDA-MB-231 lipid raft compartment (Moissoglu et al., 2014; Payapilly & Malliri, 2018). Immunoblot analysis of the active Rac1 pull-down revealed that the level of active Rac1 relative to Flotillin-1 is lower in lipid

rafts derived from p140Cap than in mock cells (Figure 9D, E). These data show that p140Cap is also a component of the lipid rafts compartment in BC cells, participating in the negative control of Rac1 activity, whose inhibition may contribute to the observed impaired cell migration in p140Cap cells.

Figure 9

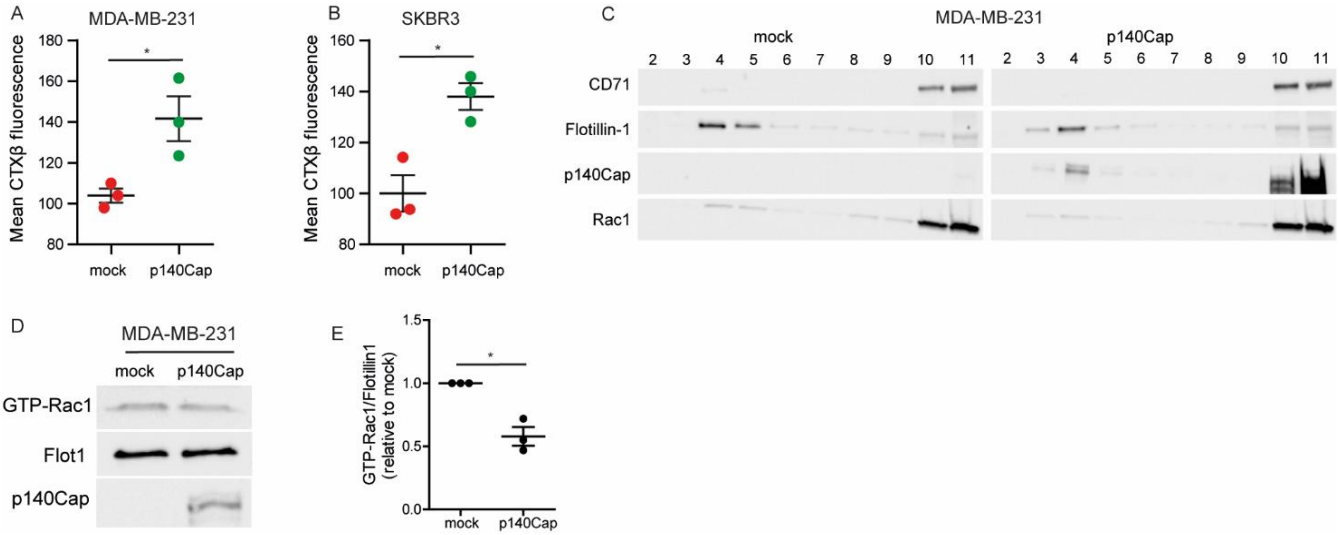

Figure 9. p140Cap downregulates Rac1 activity in lipid rafts. (A-B) mock and p140Cap MDA-MB-231 and SKBR3 cells were labeled with Alexa CTX-β and analyzed by flow cytometry. Quantification was performed considering fluorescence mean intensity for each sample. (C) Immunoblot of fractions recovered from a sucrose gradient ultracentrifuge of MDA-MB-231 cells. Triton-X 100 insoluble fractions were identified by flotillin-1, whereas TritonX-100 insoluble fractions are positive for CD71. (D) Rac1 Activation Assay performed on the lipid-raft enriched fraction (#4) of MDA-MB-231 cells. Representative immunoblot of the pull-down experiment with Rac1, western blot of flotillin-1, and p140Cap. (E) Densitometric analysis of relative GTP-Rac1 levels, normalized on flotillin-1.

4.3. Materials and Methods

Gene Ontology Analysis. Gene ontology (GO) analysis was performed on a dataset of up-regulated genes in p140Cap MDA-MB-231 cells (Sharma et al., 2013). The lists of genes were loaded on the DAVID tool for functional annotation analysis (http://david.abcc.ncifcrf.gov/summary.jsp), using the Agilent Whole Genome Oligo Microarray 8x60K as background for the upregulated genes.

Cell lines and Antibodies. Culture media were from Invitrogen (Carlsbad, CA, USA). Fetal Calf Serum (FCS) was from EuroClone (Pero, Milano, Italy). MDA-MB-231, SKBR3, and HEK293T cell lines were obtained from ATCC (LGC Standards S.r.l.—Italy Office, Italy). SKBR3 cells were cultured in McCoy's medium 15% FCS. MDA-MB-231 and HEK293t cells were cultured in DMEM 10% FCS. NeuT-TUBO cells (TUBO) were cultured in DMEM 20% FCS. Cells were maintained in media supplemented with penicillin/streptavidin. p140Cap mouse monoclonal antibody was produced in our laboratory. The following commercial antibodies were used: GAPDH (MAB374, Millipore Corp. USA), HMGCR (sc-271595, Santa Cruz Biotechnology, Santa Cruz, CA), anti-phosphoserine antibody (Sigma Chemical Co.), calreticulin (ABR Affinity Bioreagents, Thermo Scientific, Waltham, MA), mono-polyubiquitin antibody (Axxora, Lausanne, Switzerland), SREBP-2 (#557037, BD Bioscience), Flotillin-1 (sc-25506, Santa Cruz Biotechnology, Santa Cruz, CA) α-transferrin receptor-1 (CD71) (Thermo Fisher Scientific), RAC1 (from Rac1 activation assay, Cell Biolabs, Inc., San Diego, CA), HRP-conjugated cholera toxin B (SIGMA). Secondary antibodies conjugated with peroxidase were purchased from GE Healthcare.

Retroviral infection and transfections. p140Cap cDNA was cloned into a place-puro vector. The retroviruses particles were produced by the calcium phosphate transfection of Platinum Retroviral Packaging Cell Lines (Cell BioLabs), collected, filtered, and added to subconfluent SKBR3, MDA-MB-231, and TUBO cells. After

48 h, cells were washed and selected with 1 mg/ml puromycin (Sigma). Four positive clones were pooled to rule out clonal artifacts. Control cells (mock cells) were generated by using the empty vector. HEK293T cells were transfected for transient p140Cap expression by the calcium phosphate precipitation method. Transient transfections of ON-TARGET plus human SRCIN1 small-interfering RNA (siRNA) or ON-TARGET plus non-targeting siRNA (Dharmacon RNAi, GE Healthcare, Buckinghamshire, UK) were performed with Lipofectamine 2000 (Invitrogen, USA) according to manufacturer's protocol.

Western Blotting. Cells were lysed using a RIPA buffer (50mM Tris (pH 7.5), 150 mM NaCl, 1% Triton X-100, 1% Na Deoxycholate, 0.1% SDS, and protease inhibitors). Lysates were centrifuged at 13000 g for 15 min; the supernatants were collected and assayed for protein concentration using the Bio-Rad protein assay method (Biorad, Hercules, CA, USA). Proteins were run on SDS–PAGE under reducing conditions, transferred to Nitrocellulose membranes, incubated with specific antibodies, and then detected with HRP-conjugated secondary antibodies and the chemiluminescent ECL reagent.

HMGCR immunoprecipitation and activity. 10 x 10^6 cells (after overnight starvation) were rinsed with the lysis buffer (10 mM Tris, 100 mM NaCl, 20 mM KH2PO4, 30mM EDTA, 1 mM EGTA, 250 mM sucrose, pH 7.5) supplemented with protease inhibitor cocktail set III (100 mM AEBSF, 80 mM aprotinin, 5 mM bestatin, 1.5 mM E-64, 2 mM leupeptin, and 1 mM pepstatin; Merck), 1 mM Na3VO4, 1 mM NaF, 1 mM PMSF, 10 mM aprotinin and 10 mM DTT. After sonication (two bursts of 10 s; Labsonic sonicator, Sartorius Stedim Biotech S.A., Aubagne Cedex, France), cell lysates were centrifuged at 13000 x g for 15 min at 4°C. The supernatants were centrifuged at 100000 g for 1 h at 4°C, using an Optima L-90K Beckman Coulter Ultracentrifuge (Beckman Coulter Inc, Fullerton, CA) to collect the microsomal fraction, which was re-suspended in 250 µl lysis

buffer and stored at -80°C until the use. To measure HMGCR expression, 50 µg microsomal extracts were immunoprecipitated with an anti-HMGCR antibody using 25 µL of PureProteome Magnetic Beads (Millipore, Bedford, MA) in the presence of 100 mM DTT and 1 mM mevalonic acid. Western blotting was performed as described above. 10 µg microsomal proteins were probed with CRT antibody as a control of equal loading.

For the HMGCR activity assay, microsomal protein extracts were resuspended in lysis buffer (12.5 µg proteins in 25 µl), supplemented with 10 mM DTT, 5 mM NADP, and an NADPH-generating system (1.3 mM glucose 6-phosphate, 0.67 U/ml glucose-6 phosphate dehydrogenase, 33 mM $MgCl_2$). The reaction was started by adding 60 nCi [^{14}C]HMG-CoA (50–62 mCi/mmol, Amersham Bioscience). After a 20-min incubation at 37°C, the reaction was stopped with 25 µl 10 N HCl. The samples were stirred for 30 min at 37°C to ensure complete lactonization of mevalonic acid, centrifuged at 13000 x g for 2 min and separated by TLC on silica gel plates with hexane/acetone (1:1) as mobile phase. A 1 mM solution of purified mevalonolactone was used as standard. The labeled product, [^{14}C]mevalonolactone, was recovered from the TLC plates and quantified by liquid scintillation. HMGCR activity was expressed as nmol [^{14}C]mevalonolactone/mg cell proteins, according to a titration curve previously set.

***qRT–PCR*.** Total RNA was extracted using the RNeasy Mini kit (Qiagen, CA) with DNase I treatment. RT–PCR was performed on 1 µg total RNA with the High-Capacity cDNA Reverse Transcription kit from Applied Biosystems (Thermo fisher scientific). Gene expression was assessed by quantitative real-time PCR with the GeneAmp 7,500 system and Platinum® SYBR® Green qPCR SuperMix-UDG Products (Invitrogen Life Science Technologies). Each sample was tested in triplicate. The ΔΔ-Ct method was used to calculate relative fold-changes normalized against RPL32. The primers used were the following:

HMGCR (F: CCCCTCTCCAGGTGTTCACA; R: AATTGAGGTAGGTTTCATAGAGATGCT); SREBF-2 (F: CGAATTGAAAGACCTGGTCATG; R: TCCTCAGAACGCCAGACTTGT); SQLE (F: CGTGCTCCTCTTGGTACCTCAT; R: CGGTCAAGGCGGAGATTATC); CYP51A1 (F: TGCAGCCTGGCTCTTACCA; R: AGCTCTGTCCCTGCGTCTGA); RPL32A (R: TGTGAGCGATCTCGGCAC; F: TTCCTGGTCCACAACAACGTCAAG); HMGCS1 (F: GGGCAGGGCATTATTAGGCTAT; R: TTAGGTTGTCAGCCTCTATGTTGAA); MVK (F: TGGACCTCAGCTTACCCAACA; R: GACTGAAGCCTGGCCACATC); PMVK (F: CCGCGTGTCTCACCCTTT; R: GACCGTGCCCTCAGCTCAT); MVD (F: TGAACTCCGCGTGCTCATC; R: CGGTACTGCCTGTCAGCTTCT); IDI1 (F: TTTCCAGGTTGTTTTACGAATACG; R: TCCTCAAGCTCGGCTGGAT); FDPS (F: CTTCCTATAGCTGCAGCCATGTAC; R: GCATTGGCGTGCTCCTTCT); FDFT1 (F: TCAGACCAGTCGCAGTTTCG; R: CTGCGTTGCGCATTTCC); LSS (F: TGCAGAAGGCTCATGAGTTCCT; R: TCTGGTAGTCGGGAGGGTTATC); TM7SF2 (F: GCCACCCTCACCGCTTT; R: GCTACCTGCGCCTTCATGTAG); SC4MOL (F: GAAAAGCCGGCACCAAGA; R: TCAAAGAGAGAATCAGCTCAAACTG); NSDHL (F: AGAATCAGGCCAAGAGATGCA; R: TGTGCTGCCCCAGGAATC); DHCR7 (F: GGCATCCCAGCTCCAACTC; R: GGGCTCTCTCCAGTTTACAGATGA); DHCR24 (F: CAAGTACGGCCTGTTCCAACA; R: CGCACAAAGCTGCCATCA).

Luciferase Assay. The pLDLR-Luc plasmid (Addgene #14940) harboring the SREBP-responsive Sterol Regulatory Element (SRE) sequence (ATCACCCCAC) and the pLDLR-Luc mutSRE construct (Addgene #14945) containing the SREBP-unresponsive mutant SRE (ATAACCCCAC) were gifts from Giannino del Sal. pLDLR-Luc (208 ng/cm2) or pLDLR-Luc mutSRE (208 ng/cm2) plasmids were co-transfected with CMV-Renillia (93 ng/cm2) and p140Cap-MYC (208 ng/cm2) plasmids in Hek293t cells by using the Calcium Phosphate transfection method. MYC (125 ng/cm2) construct instead of p140Cap-MYC was used as a negative control. 24 h after transfection, the Firefly/Renilla signal was analyzed in cell lysates using the Dual-Luciferase Reporter Assay System (Promega E1910). The

experiment was performed in three biological replicates and four technical replicates, each in a 96-well plate.

MVA pathway metabolic flux. Cells were labeled with 1 µCi/ml [^{3}H]acetate (3600 mCi/mmol; Amersham Bioscience, Piscataway, NJ), and the synthesis of radiolabeled cholesterol, geranylgeranyl pyrophosphate, and ubiquinone were measured as described in Campia et al. (Campia et al., 2009). After 24 h, the cells were washed twice with phosphate-buffered saline (PBS) and mechanically scraped in 200 µl of PBS. 500 µl of methanol and 1 ml of hexane were added to the cell suspension, which was stirred at room temperature for 1 h and then centrifuged at 2000 × g for 5 min. The upper phase containing hexane was transferred into a new test tube, and the lower phase was supplemented with 1 ml of hexane and stirred overnight. After a 5 min centrifugation at 2000 × g, the upper phase was added to the previous one, and the solvent was allowed to evaporate at room temperature for 24 h. Cellular lipid extracts produced by this separation were re-suspended in 30 µl of chloroform and then subjected to thin layer chromatography (TLC), using a 1:1 (v/v) ether/hexane solution as mobile phase. Each sample was spotted on pre-coated LK6D Whatman silica gels (Merck, Darmstadt, Germany) and allowed to run for 30 min. Solutions of 10 µg/ml cholesterol were used as standard. The silica gel plates were exposed for 1 h to an iodine-saturated atmosphere. The migrated spots were cut out, and their radioactivity was measured by liquid scintillation using a Tri-Carb Liquid Scintillation Analyzer (PerkinElmer, Waltham, MA). Cholesterol, GGPP, and ubiquinone synthesis were expressed as fmoles/10^6 cells, according to previously prepared titration curves. When MVA pathway inhibitors (simvastatin [12], zoledronic acid [13], and squalestatin were used, cells were treated for 24 h before incubating with [^{3}H]acetate.

Cholesterol depletion, loading, and intracellular cholesterol measurement. To prepare cholesterol/MβCD complexes, cholesterol was dissolved in 2-propanol/chloroform 2:1 (v/v) at a final concentration of 6.5 mM and added to an aqueous solution of 66.7 mM MβCD previously heated at 80°C for 20 min. During the overnight evaporation of the solvent, cholesterol is progressively associated with MβCD in a soluble mixture. In cholesterol loading assays, 5 x 106 cells (after overnight starvation) were incubated with 0.67 mM MβCD for 4 h, then washed; fresh medium containing 0.5 mM cholesterol/MβCD complexes was added for 24 h. In cholesterol depletion assays, cells were incubated with 0.67 mM MβCD for 4 h. Then, the intracellular cholesterol was measured using the Cholesterol Fluorimetric Assay kit (Cayman Chemical, Ann Arbor, MI) as per the manufacturer's instructions. Results were expressed as µmol cholesterol/mg cell proteins.

Cholesterol efflux. To evaluate cholesterol efflux, 1 x 10^6 cells (after overnight starvation) were incubated with 1 µCi/ml [^{3}H]cholesterol (Amersham Bioscience) for 1 h, washed five times with PBS, and grown in a fresh medium for 24 h. The cell culture medium was collected, and cholesterol was extracted in methanol-hexane and resolved by TLC. The amount of [^{3}H]cholesterol recovered was quantified by liquid scintillation and expressed as fmol/10^6 cells, according to the titration curve prepared previously. Results were expressed as percentages towards mock/control cells.

ABC transporter activity. To prepare plasma-membrane vesicles enriched with ATP-binding cassette transporters, 10 x 10^6 cells (after overnight starvation) were washed with Ringer's solution (148.7 mM NaCl, 2.55 mM K_2HPO_4, 0.45 mM KH_2PO_4, 1.2 mM $MgSO_4$; pH 7.4), lysed on crushed ice with lysis buffer (10 mM Hepes/Tris, 5 mM EDTA, 5 mM EGTA, 2 mM DTT; pH 7.4) supplemented with 2 mM PMSF, 1 mM aprotinin, 10 µg/mL pepstatin, 10 µg/mL leupeptin, and

subjected to nitrogen cavitation at 1200 psi for 20 min. Samples were centrifuged at 300 x g for 10 min, diluted 1:4 in the pre-centrifugation buffer (10 mM Tris/HCl, 25 mM sucrose; pH 7.5), overlaid on a sucrose cushion (10 mM Tris/HCl, 35% w/v sucrose, 1 mM EDTA; pH 7.5) and centrifuged at 14000 x g for 10 min. The interface was collected, diluted 1:5 in the centrifugation buffer (10 mM Tris/HCl, 250 mM sucrose; pH 7.5), and subjected to a third centrifugation at 100000 x g for 45 min (Optima L-90K Beckman Coulter Ultracentrifuge). The vesicle pellet was resuspended in 0.5 ml centrifugation buffer and stored at -80°C until use after quantifying the protein content. 100 µg proteins were immunoprecipitated in non-denaturing conditions using anti-ABCA1 (diluted 1:100, mouse clone HJI, Abcam, Cambridge, UK) and anti-ABCG1 (diluted 1:100, rabbit polyclonal, #NB400-132, Novus Biologicals, Littleton, CO) antibodies, in the presence of 25 µL of PureProteome Magnetic Beads. The ATPase activity of immunopurified ABCA1 and ABCG1 was measured by a spectrophotometric method: samples (containing 20 µg proteins) were incubated for 30 min at 37°C with 50 µl of the reaction mix (25 mM Tris/HCl, 3 mM ATP, 50 mM KCl, 2.5 mM $MgSO_4$, 3 mM DTT, 0.5 mM EGTA, 2 mM ouabain, 3 mmol/L NaN_3; pH 7.0). A blank containing 0.5 mM Na_3VO_4 was included in each set of experiments. The reaction was stopped by adding 0.2 ml ice-cold stopping buffer (0.2% w/v ammonium molybdate, 1.3% v/v H_2SO_4, 0.9% w/v SDS, 2.3% w/v trichloroacetic acid, 1% w/v ascorbic acid). After a 30-min incubation at room temperature, the absorbance of the phosphate hydrolyzed from ATP was measured at 620 nm using a Packard EL340 microplate reader (Bio-Tek Instruments, Winooski, MA). The absorbance was converted into µmol hydrolyzed phosphate/min/mg proteins, according to the titration curve previously prepared. The ATPase activity was expressed as a percentage of mock/control cells.

Membrane cholesterol measurement. 10 x 10^6 cells were lysed in 0.5 mL of 10 mM Tris, 100 mM NaCl, 20 mM KH_2PO_4, 30mM EDTA, 1 mM EGTA, 250 mM

sucrose, pH 7.5, and sonicated with 2 bursts of 10 s (Labsonic sonicator, Sartorius Stedim Biotech S.A., Aubagne Cedex, France), then centrifuged at 13000 x g for 15 min at 4°C. The supernatants were centrifuged at 100000 g for 1 h at 4°C, using an Optima L-90K Beckman Coulter Ultracentrifuge (Beckman Coulter Inc, Fullerton, CA) to collect the membrane fractions. The pellets were resuspended in 250 µL of the assay buffer provided by fluorimetric Cholesterol/Cholesteryl Ester Assay Kit – Quantitation (Abcam) and used to measure free cholesterol in the membrane, as per manufacturer's instructions. An aliquot of 50 µl was sonicated again to measure the membrane proteins. Results were expressed as mg cholesterol/mg membrane proteins.

Membrane Fluidity Measurement. Membrane fluidity was measured in triplicate using a membrane fluidity kit (Marker Gene Technologies M0271) according to the manufacturer's protocol.

Wound Healing migration assays. *C*ells were allowed to grow at the confluence. Upon scratch using a 200 µl tip, cells were PBS washed twice and maintained in a serum-free medium. Images were acquired with ×10 objective Carl Zeiss microscope. The wound area was calculated with Fiji software. Three replicate wells for each condition were analyzed in at least 3 independent experiments.

Lipid rafts flow-cytometer analysis. $1x10^6$ cells were PBS washed, incubated with 1 µg CTX-β Alexa Fluor-488 Conjugate (CTX-β 488, ThermoFisher) diluted in PBS for 15 minutes at 4°C, rewashed in PBS and analyzed by flow cytometry. At least 10,000 events/samples were acquired by the FACSCalibur cytometer (BD Biosciences). Data analysis was performed by gating living cells, excluding death cells and debris, and subtracting the fluorescence of unlabelled cells.

Lipid rafts isolation. Lipid rafts were isolated as described in Rodgers and Rose (Rodgers & Rose, 1996). Briefly, 100 x 10^6 cells were lysed with 1% TritonX-100 Lysis Buffer (10 mM Tris-HC1 pH 7.5, 150 mM NaCl, 5 mM EDTA, 1 mM Na_3VO_4, and proteases inhibitors) and Dounce homogenized. Lysates were centrifuged for 5 min at 1300 g for nuclei and debris removal. For equilibrium centrifugation, cleared lysates were diluted in an SW41 centrifuge tube with an equal volume of 85% wt/vol sucrose in TNEV (10 mM Tris-HC1 pH 7.5, 150 mM NaCl, 5 mM EDTA, and 1 mM Na_3VO_4), overlaid with 6 ml of 30% wt/vol and 3.5 ml 5% wt/vol sucrose solutions in TNEV. Samples were centrifuged for 17h at 200000 g at 4°C with no brake during the deceleration phase. Eleven 1 ml fractions were collected and tested for GM1 positivity by CTX-β staining in a dot blot assay. Specifically, 1 uL of each fraction was dot blotted onto nitrocellulose, blocked with 5% BSA TBS-Tween, and incubated with HRP-conjugated CTX-β for 30 min. After two washes with TBS, dots were revealed with the chemiluminescence method. Gradient fractions positive for CTX-β and Flotillin-1 were further assessed for Rac1 activity with the Rac1 activation assay (Cell Biolabs, Inc., San Diego, CA) according to the manufacturer's instructions.

Statistical analysis. Prism software (GraphPad) was used for statistical analysis. Significance was calculated with a Student t test and one- or two-way analysis of variance tests (ANOVA) followed by Bonferroni's post hoc analysis. Data are reported as mean ± SEM.

4.4. Discussion

The role of cholesterol metabolism in BC development is still controversial since human studies have failed to provide a consensus regarding the association between cholesterol and BC (Centonze, Natalini, Piccolantonio, et al., 2022; Guerra et al., 2021; Nazih & Bard, 2020). In this work, we identify the p140Cap adaptor protein as a new player in controlling the MVA pathway and cholesterol metabolism, affecting BC cell migration.

We demonstrated that cells expressing p140Cap show increased synthesis of the MVA pathway intermediates by the upregulation of the enzyme catalyzing the rate-limiting step of the pathway, HMGCR, at both transcriptional and post-translational levels. p140Cap exerts this effect on the MVA pathway in Her2-amplified (SKBR3, TUBO) and in triple-negative (MDA-MB-231) BC cellular models, suggesting a general role of p140Cap in different molecular BC subtypes. Interestingly, the transient expression of p140Cap in the heterologous system of HEK293T cells leads to a similar upregulation of the MVA pathway, indicating that even transient p140Cap expression is sufficient to modulate the MVA pathway also in non-BC cells. By targeting the MVA pathway with simvastatin, the production of cholesterol, GGPP, and ubiquinone was significantly reduced, suggesting that p140Cap acts upstream of the HMGCR activity.

Our data excluded the involvement of p140Cap in the AMPK-mediated control of the HMGCR (Clarke & Hardie, 1990). Importantly, we observed increased HMGCR mRNA levels in p140Cap cells, likely due to the increased transcriptional control by the SREBP2 transcription factor, as revealed by luciferase assay. It has been shown that mutant p53 associates with SREBP2 and upregulates HMGCR and other MVA genes in BC cells, making the cells highly dependable on the flux through the MVA pathway and sensitive to its inhibition (Freed-Pastor et al., 2012). The human breast cancer cells used in our work harbor different missense mutations of p53 (p.R280K for MDA-MB-231 and p.R175H for SKBR3) (https://www.atcc.org/, https://cancer.sanger.ac.uk/cell_lines). However, we

observed that the increased metabolic flux through the MVA pathway by p140Cap is also present in HEK293t cells that harbor a wt-p53 form of p53. Thus, our data strongly suggest that p140Cap exerts a mechanism of control of the MVA pathway independently on mutant p53 activity.

In physiological conditions, cells modulate SREBP2 maturation and HMGCR ubiquitination according to the intracellular cholesterol levels sensed in the endoplasmic reticulum (ER) (Guerra et al., 2021; Xue et al., 2020). Specifically, low cholesterol levels in the ER initiate a feedback mechanism leading to SREBP2 activation and reduced ubiquitin-dependent HMGCR degradation, thus increasing cholesterol biosynthesis. Notably, HMGCR is less ubiquitinated in p140Cap cells than in mock cells, leading to increased protein stability, indicating that p140Cap tunes HMGCR levels at both transcriptional and post-translational levels. For this reason, we speculate that p140Cap cells might sense low cholesterol levels in the ER, promoting the dual control mechanisms of HMGCR. However, the exact molecular mechanisms underlying p140cap-mediated regulation of HMGCR and SREBP2 need to be clarified.

In literature, it is reported that cholesterol synthesis is upregulated in several malignancies, including BC (Guerra et al., 2021; Nazih & Bard, 2020), since it is mainly used as a building block for proliferating cells. Consequently, the observed effect of p140Cap on enhanced cholesterol synthesis appears to point to a pro-tumorigenic impact, in contrast with the previously described role of p140Cap as an anti-cancer protein (Grasso et al., 2020; Grasso et al., 2017). However, we found that the increased newly synthesized cholesterol in p140Cap cells does not accumulate in the cells. Still, it is either rapidly extruded by ABC transporters or differently distributed in specific cellular compartments.

Our data suggest that the enhanced outflow from the cells is due to a homeostatic mechanism to keep an adequate intracellular cholesterol concentration. In particular, we showed that both ABCA1 and ABCG1 transporters were more active in p140Cap cells. However, further investigation is required to deeply

assess the direct or indirect interaction between p140Cap and these transmembrane proteins.

Moreover, we demonstrated that in p140Cap cell lines, there is a different distribution of cellular cholesterol. Specifically, we observed an increased cholesterol content in the plasma membrane of p140Cap cells, leading to reduced membrane fluidity and an impaired cell migration ability. Indeed, by loading mock cells with cholesterol, we decreased membrane fluidity to the same extent as p140Cap cells, leading to reduced cell migration. Our data are consistent with previous studies showing that reduced cholesterol in the membrane in triple-negative breast cancer (TNBC) cells is associated with increased metastatic potential (Wang et al., 2022). In contrast, higher cholesterol content resulting from enhanced de novo biosynthesis leads to increased rigidity and reduced fluidity, thus contributing to decreased mobility of malignant cells (Zeisig et al., 2007; Zhao et al., 2016).

Cholesterol is pivotal in lipid rafts organization, stabilization, and signaling events (Vona et al., 2021). Lipid rafts are small, heterogeneous, and highly dynamic membrane microdomains enriched in the saturated photo-, sphingo- and glycolipids, cholesterol, lipidated proteins, and glycosylphosphatidylinositol (GPI)-anchored proteins. Lipid rafts increased lipid packing and order and decreased fluidity. Moreover, these membrane micro-domains are resistant to solubilization by non-ionic detergents (i.e., TritonX-100) at cold temperatures, allowing the membrane fractionation of cellular membranes into detergent-soluble membrane fractions and detergent-resistant membrane fractions (Rodgers & Rose, 1996). Lipid rafts participate in cellular processes, including membrane trafficking, regulation of membrane protein activity, and the control of signal transduction events, mainly by compartmentalizing different signaling molecules (Mollinedo & Gajate, 2020; Sezgin et al., 2017). Notably, we recently demonstrated how p140Cap controls protein localization in the neurons' lipid raft membrane compartment (Angelini et al., 2022). Here, we show that p140Cap is

associated with lipid rafts also in BC cells, likely functioning as a signaling platform in this compartment. p140Cap can negatively control the activity of the Rac1 GEF Tiam1 (Chapelle et al., 2020). In this work, we demonstrated that p140Cap reduces Rac1 activity in lipid rafts of MDA-MB-231 cells, indicating that p140Cap might interact with Rac1 GTPase regulators in the lipid raft compartment.

Overall, our findings revealed new roles for p140Cap in BC cells, namely its ability to regulate the MVA pathway and cellular cholesterol distribution, impacting tumor cell properties such as cell migration.

5. Conclusions

This work unveiled new functions for the adaptor proteins p130Cas and p140Cap in cancer, investigating PDAC initiation and BC cholesterol metabolism, respectively. Although we studied two different cancers and biological processes, we already know from our previous work that p130Cas and p140Cap may exert opposite activities in BC, impinging on specific signaling pathways. Rac1 and Src are putative points of crosstalk in which p130Cas and p140Cap may exert their antagonistic functions in the regulation of tumorigenic signaling. Indeed, Rac1 GTPase is kept inactive by p140Cap through the inhibition of the GEF Tiam1, whereas the assembly of the p130Cas/DOCK180 complex induces the recruitment of active Rac1 to the cell membrane. Moreover, the p140Cap/CSK and p130Cas/FAK interactions contribute to the inhibition and activation of Src activity, respectively (Figure 10, (Centonze, Natalini, Salemme, Costamagna et al. ,2021)). The fact that the two proteins have common interacting partners, such as the Src kinase, with opposite effects further indicates that the two proteins share a common network and that temporal analysis of their reciprocal localization and kinetics of interactions with specific interactors would be of great interest to shed light on their function. While the pro-survival, proliferative, and invasive functions of p130Cas have been extensively investigated in various malignancies, little is known about its putative involvement in the metabolic alterations of cancer cells. Future experiments could address the possible interactions of p130Cas and p140Cap in the context of BC cholesterol metabolism. Likewise, the potential involvement of p140Cap in PDAC carcinogenesis has never been explored. Nevertheless, it has been reported that p140Cap is enriched in the pancreatic α- and β- cells of the rat pancreas, whereby it could modulate insulin secretion (Yamauchi et al., 2013), suggesting a potential role for p140Cap in PDAC.

Understanding the nature and the functional role of the multi-protein complexes associated with p140Cap and p130Cas adaptor proteins might be critical to

discover new biologically relevant and potentially targetable pathways in the context of breast cancer. The generation of a protein-protein interaction network could help achieve this goal. A recent comprehensive analysis of p140Cap interactome in BC TUBO cells has provided insights into its involvement in new putative biological networks relevant to cancer progression (Chapelle et al., 2019). The study uncovered 373 interacting proteins, among which molecules whose functions are frequently deregulated in cancer, such as cell-substrate junction, cell-cell adhesion, protein homeostasis, regulation of cell cycle, and apoptosis. Therefore, it would be of great interest to gain insights into the p130Cas and p140Cap interactomes in breast cancer and pancreatic cells, respectively, which would allow a better understanding of the putative interaction and opposing contributions of p140Cap and p130Cas adaptor proteins in controlling cancer cell signaling pathways.

Moreover, the genetically modified mice in which either p130Cas or p140Cap can be specifically ablated in a specific tissue (Del Pilar Camacho Leal et al., 2018; Russo et al., 2019; Costamagna, Natalini, et al., 2022) could be exploited to further address the impact of each protein in physiological development or in tumor progression, focusing on the functional balance of the common network of interacting proteins.

Figure 10

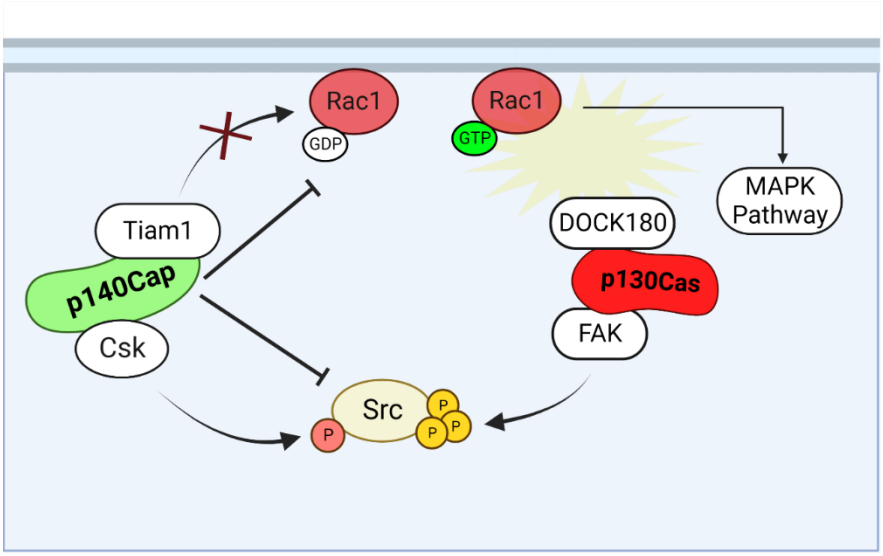

Figure 10. Putative p130Cas and p140Cap points of crosstalk in breast cancer (Centonze, Natalini, Salemme, Costamagna, et al., 2021). Rac1 and Src are the possible points of crosstalk in which p130Cas and p140Cap may exert their antagonistic functions in the regulation of tumorigenic signaling. While Rac1 GTPase is kept inactive by p140Cap through the inhibition of the GEF Tiam1, the assembly of p130Cas/DOCK180 complex induces the recruitment of active Rac1 to the cell membrane. The p140Cap/CSK and p130Cas/FAK interactions contribute to the inhibition and activation of Src activity, respectively.

6. Bibliography

Alikhani, N., Ferguson, R. D., Novosyadlyy, R., Gallagher, E. J., Scheinman, E. J., Yakar, S., & LeRoith, D. (2013). Mammary tumor growth and pulmonary metastasis are enhanced in a hyperlipidemic mouse model. *Oncogene*, *32*(8), 961-967. https://doi.org/10.1038/onc.2012.113

Angelini, C., Morellato, A., Alfieri, A., Pavinato, L., Cravero, T., Bianciotto, O. T., Salemme, V., Natalini, D., Centonze, G., Raspanti, A., Garofalo, T., Valdembri, D., Serini, G., Marcantoni, A., Becchetti, A., Giustetto, M., Turco, E., & Defilippi, P. (2022). p140Cap regulates the composition and localization of the NMDAR complex in synaptic lipid rafts. *J Neurosci*, *42*(38), 7183-7200. https://doi.org/10.1523/jneurosci.1775-21.2022

Ardito, C. M., Grüner, B. M., Takeuchi, K. K., Lubeseder-Martellato, C., Teichmann, N., Mazur, P. K., Delgiorno, K. E., Carpenter, E. S., Halbrook, C. J., Hall, J. C., Pal, D., Briel, T., Herner, A., Trajkovic-Arsic, M., Sipos, B., Liou, G. Y., Storz, P., Murray, N. R., Threadgill, D. W., . . . Siveke, J. T. (2012). EGF receptor is required for KRAS-induced pancreatic tumorigenesis. *Cancer Cell*, *22*(3), 304-317. https://doi.org/10.1016/j.ccr.2012.07.024

Baek, A. E., Yu, Y. A., He, S., Wardell, S. E., Chang, C. Y., Kwon, S., Pillai, R. V., McDowell, H. B., Thompson, J. W., Dubois, L. G., Sullivan, P. M., Kemper, J. K., Gunn, M. D., McDonnell, D. P., & Nelson, E. R. (2017). The cholesterol metabolite 27 hydroxycholesterol facilitates breast cancer metastasis through its actions on immune cells. *Nat Commun*, *8*(1), 864. https://doi.org/10.1038/s41467-017-00910-z

Baer, R., Cintas, C., Dufresne, M., Cassant-Sourdy, S., Schönhuber, N., Planque, L., Lulka, H., Couderc, B., Bousquet, C., Garmy-Susini, B., Vanhaesebroeck, B., Pyronnet, S., Saur, D., & Guillermet-Guibert, J. (2014). Pancreatic cell plasticity and cancer initiation induced by oncogenic Kras is completely dependent on wild-type PI 3-kinase p110α. *Genes Dev*, *28*(23), 2621-2635. https://doi.org/10.1101/gad.249409.114

Bailey, J. M., DelGiorno, K. E., & Crawford, H. C. (2014). The secret origins and surprising fates of pancreas tumors. *Carcinogenesis*, *35*(7), 1436-1440. https://doi.org/10.1093/carcin/bgu056

Bertolio, R., Napoletano, F., Mano, M., Maurer-Stroh, S., Fantuz, M., Zannini, A., Bicciato, S., Sorrentino, G., & Del Sal, G. (2019). Sterol regulatory element binding protein 1 couples mechanical cues and lipid metabolism. *Nat Commun*, *10*(1), 1326. https://doi.org/10.1038/s41467-019-09152-7

Bill, R., & Christofori, G. (2015). The relevance of EMT in breast cancer metastasis: Correlation or causality? *FEBS Lett*, *589*(14), 1577-1587. https://doi.org/10.1016/j.febslet.2015.05.002

Bisaro, B., Sciortino, M., Colombo, S., Camacho Leal, M. P., Costamagna, A., Castellano, I., Montemurro, F., Rossi, V., Valabrega, G., Turco, E., Defilippi,

P., & Cabodi, S. (2016). p130Cas scaffold protein regulates ErbB2 stability by altering breast cancer cell sensitivity to autophagy. *Oncotarget*, *7*(4), 4442-4453. https://doi.org/10.18632/oncotarget.6710

Blasco, M. T., Navas, C., Martín-Serrano, G., Graña-Castro, O., Lechuga, C. G., Martín-Díaz, L., Djurec, M., Li, J., Morales-Cacho, L., Esteban-Burgos, L., Perales-Patón, J., Bousquet-Mur, E., Castellano, E., Jacob, H. K. C., Cabras, L., Musteanu, M., Drosten, M., Ortega, S., Mulero, F., . . . Barbacid, M. (2019). Complete Regression of Advanced Pancreatic Ductal Adenocarcinomas upon Combined Inhibition of EGFR and C-RAF. *Cancer Cell*, *35*(4), 573-587.e576. https://doi.org/10.1016/j.ccell.2019.03.002

Brindisi, M., Fiorillo, M., Frattaruolo, L., Sotgia, F., Lisanti, M. P., & Cappello, A. R. (2020). Cholesterol and Mevalonate: Two Metabolites Involved in Breast Cancer Progression and Drug Resistance through the ERRα Pathway. *Cells*, *9*(8). https://doi.org/10.3390/cells9081819

Burg, J. S., & Espenshade, P. J. (2011). Regulation of HMG-CoA reductase in mammals and yeast. *Prog Lipid Res*, *50*(4), 403-410. https://doi.org/10.1016/j.plipres.2011.07.002

Cabodi, S., del Pilar Camacho-Leal, M., Di Stefano, P., & Defilippi, P. (2010). Integrin signalling adaptors: not only figurants in the cancer story. *Nat Rev Cancer*, *10*(12), 858-870. https://doi.org/10.1038/nrc2967

Cabodi, S., Tinnirello, A., Bisaro, B., Tornillo, G., del Pilar Camacho-Leal, M., Forni, G., Cojoca, R., Iezzi, M., Amici, A., Montani, M., Eva, A., Di Stefano, P., Muthuswamy, S. K., Tarone, G., Turco, E., & Defilippi, P. (2010). p130Cas is an essential transducer element in ErbB2 transformation. *Faseb j*, *24*(10), 3796-3808. https://doi.org/10.1096/fj.10-157347

Camacho Leal Mdel, P., Sciortino, M., Tornillo, G., Colombo, S., Defilippi, P., & Cabodi, S. (2015). p130Cas/BCAR1 scaffold protein in tissue homeostasis and pathogenesis. *Gene*, *562*(1), 1-7. https://doi.org/10.1016/j.gene.2015.02.027

Camacho Leal, M. D. P., Costamagna, A., Tassone, B., Saoncella, S., Simoni, M., Natalini, D., Dadone, A., Sciortino, M., Turco, E., Defilippi, P., Calautti, E., & Cabodi, S. (2018). Conditional ablation of p130Cas/BCAR1 adaptor protein impairs epidermal homeostasis by altering cell adhesion and differentiation. *Cell Commun Signal*, *16*(1), 73. https://doi.org/10.1186/s12964-018-0289-z

Campia, I., Gazzano, E., Pescarmona, G., Ghigo, D., Bosia, A., & Riganti, C. (2009). Digoxin and ouabain increase the synthesis of cholesterol in human liver cells. *Cell Mol Life Sci*, *66*(9), 1580-1594. https://doi.org/10.1007/s00018-009-9018-5

Cancer Stat Facts: Pancreatic Cancer. https://seer.cancer.gov/statfacts/html/pancreas.html

Carrer, A., Trefely, S., Zhao, S., Campbell, S. L., Norgard, R. J., Schultz, K. C., Sidoli, S., Parris, J. L. D., Affronti, H. C., Sivanand, S., Egolf, S., Sela, Y., Trizzino, M., Gardini, A., Garcia, B. A., Snyder, N. W., Stanger, B. Z., & Wellen, K. E.

(2019). Acetyl-CoA Metabolism Supports Multistep Pancreatic Tumorigenesis. *Cancer Discov*, *9*(3), 416-435. https://doi.org/10.1158/2159-8290.Cd-18-0567

Castellano, E., & Downward, J. (2011). RAS Interaction with PI3K: More Than Just Another Effector Pathway. *Genes Cancer*, *2*(3), 261-274. https://doi.org/10.1177/1947601911408079

Centonze, G., Natalini, D., Piccolantonio, A., Salemme, V., Morellato, A., Arina, P., Riganti, C., & Defilippi, P. (2022). Cholesterol and Its Derivatives: Multifaceted Players in Breast Cancer Progression. *Front Oncol*, *12*, 906670. https://doi.org/10.3389/fonc.2022.906670

Centonze, G., Natalini, D., Salemme, V., Costamagna, A., Cabodi, S., & Defilippi, P. (2021). p130Cas/BCAR1 and p140Cap/SRCIN1 Adaptors: The Yin Yang in Breast Cancer? *Front Cell Dev Biol*, *9*, 729093. https://doi.org/10.3389/fcell.2021.729093

Chapelle, J., Baudino, A., Torelli, F., Savino, A., Morellato, A., Angelini, C., Salemme, V., Centonze, G., Natalini, D., Gai, M., Poli, V., Kähne, T., Turco, E., & Defilippi, P. (2020). The N-terminal domain of the adaptor protein p140Cap interacts with Tiam1 and controls Tiam1/Rac1 axis. *Am J Cancer Res*, *10*(12), 4308-4324.

Chapelle, J., Sorokina, O., McLean, C., Salemme, V., Alfieri, A., Angelini, C., Morellato, A., Adrait, A., Menna, E., Matteoli, M., Couté, Y., Ala, U., Turco, E., Defilippi, P., & Armstrong, J. D. (2019). Dissecting the Shared and Context-Dependent Pathways Mediated by the p140Cap Adaptor Protein in Cancer and in Neurons. *Front Cell Dev Biol*, *7*, 222. https://doi.org/10.3389/fcell.2019.00222

Childs, E. J., Mocci, E., Campa, D., Bracci, P. M., Gallinger, S., Goggins, M., Li, D., Neale, R. E., Olson, S. H., Scelo, G., Amundadottir, L. T., Bamlet, W. R., Bijlsma, M. F., Blackford, A., Borges, M., Brennan, P., Brenner, H., Bueno-de-Mesquita, H. B., Canzian, F., . . . Klein, A. P. (2015). Common variation at 2p13.3, 3q29, 7p13 and 17q25.1 associated with susceptibility to pancreatic cancer. *Nat Genet*, *47*(8), 911-916. https://doi.org/10.1038/ng.3341

Chimento, A., Casaburi, I., Avena, P., Trotta, F., De Luca, A., Rago, V., Pezzi, V., & Sirianni, R. (2018). Cholesterol and Its Metabolites in Tumor Growth: Therapeutic Potential of Statins in Cancer Treatment. *Front Endocrinol (Lausanne)*, *9*, 807. https://doi.org/10.3389/fendo.2018.00807

Chin, L. S., Nugent, R. D., Raynor, M. C., Vavalle, J. P., & Li, L. (2000). SNIP, a novel SNAP-25-interacting protein implicated in regulated exocytosis. *J Biol Chem*, *275*(2), 1191-1200. https://doi.org/10.1074/jbc.275.2.1191

Clarke, P. R., & Hardie, D. G. (1990). Regulation of HMG-CoA reductase: identification of the site phosphorylated by the AMP-activated protein kinase in vitro and in intact rat liver. *Embo j*, *9*(8), 2439-2446. https://doi.org/10.1002/j.1460-2075.1990.tb07420.x

Costamagna, A., Natalini, D., Camacho Leal, M. D. P., Simoni, M., Gozzelino, L., Cappello, P., Novelli, F., Ambrogio, C., Defilippi, P., Turco, E., Giovannetti, E., Hirsch, E., Cabodi, S., & Martini, M. (2022). Docking Protein p130Cas Regulates Acinar to Ductal Metaplasia During Pancreatic Adenocarcinoma Development and Pancreatitis. *Gastroenterology*, *162*(4), 1242-1255.e1211. https://doi.org/10.1053/j.gastro.2021.12.242

Daday, C., de Buhr, S., Mercadante, D., & Gräter, F. (2022). Mechanical force can enhance c-Src kinase activity by impairing autoinhibition. *Biophys J*, *121*(5), 684-691. https://doi.org/10.1016/j.bpj.2022.01.028

Dai, Y., Qi, L., Zhang, X., Li, Y., Chen, M., & Zu, X. (2011). CrkI and p130(Cas) complex regulates the migration and invasion of prostate cancer cells. *Cell Biochem Funct*, *29*(8), 625-629. https://doi.org/10.1002/cbf.1797

Damiano, L., Di Stefano, P., Camacho Leal, M. P., Barba, M., Mainiero, F., Cabodi, S., Tordella, L., Sapino, A., Castellano, I., Canel, M., Frame, M., Turco, E., & Defilippi, P. (2010). p140Cap dual regulation of E-cadherin/EGFR cross-talk and Ras signalling in tumour cell scatter and proliferation. *Oncogene*, *29*(25), 3677-3690. https://doi.org/10.1038/onc.2010.128

Defilippi, P., Di Stefano, P., & Cabodi, S. (2006). p130Cas: a versatile scaffold in signaling networks. *Trends Cell Biol*, *16*(5), 257-263. https://doi.org/10.1016/j.tcb.2006.03.003

Di Stefano, P., Cabodi, S., Boeri Erba, E., Margaria, V., Bergatto, E., Giuffrida, M. G., Silengo, L., Tarone, G., Turco, E., & Defilippi, P. (2004). P130Cas-associated protein (p140Cap) as a new tyrosine-phosphorylated protein involved in cell spreading. *Mol Biol Cell*, *15*(2), 787-800. https://doi.org/10.1091/mbc.e03-09-0689

Di Stefano, P., Damiano, L., Cabodi, S., Aramu, S., Tordella, L., Praduroux, A., Piva, R., Cavallo, F., Forni, G., Silengo, L., Tarone, G., Turco, E., & Defilippi, P. (2007). p140Cap protein suppresses tumour cell properties, regulating Csk and Src kinase activity. *Embo j*, *26*(12), 2843-2855. https://doi.org/10.1038/sj.emboj.7601724

Di Stefano, P., Leal, M. P., Tornillo, G., Bisaro, B., Repetto, D., Pincini, A., Santopietro, E., Sharma, N., Turco, E., Cabodi, S., & Defilippi, P. (2011). The adaptor proteins p140CAP and p130CAS as molecular hubs in cell migration and invasion of cancer cells. *Am J Cancer Res*, *1*(5), 663-673.

dos Santos, C. R., Domingues, G., Matias, I., Matos, J., Fonseca, I., de Almeida, J. M., & Dias, S. (2014). LDL-cholesterol signaling induces breast cancer proliferation and invasion. *Lipids Health Dis*, *13*, 16. https://doi.org/10.1186/1476-511x-13-16

Eser, S., Reiff, N., Messer, M., Seidler, B., Gottschalk, K., Dobler, M., Hieber, M., Arbeiter, A., Klein, S., Kong, B., Michalski, C. W., Schlitter, A. M., Esposito, I., Kind, A. J., Rad, L., Schnieke, A. E., Baccarini, M., Alessi, D. R., Rad, R., . . . Saur, D. (2013). Selective requirement of PI3K/PDK1 signaling for Kras oncogene-driven pancreatic cell plasticity and cancer. *Cancer Cell*, *23*(3), 406-420. https://doi.org/10.1016/j.ccr.2013.01.023

Faulkner, R., & Jo, Y. (2022). Synthesis, function, and regulation of sterol and nonsterol isoprenoids. *Front Mol Biosci*, *9*, 1006822. https://doi.org/10.3389/fmolb.2022.1006822

Flynn, D. C. (2001). Adaptor proteins. *Oncogene*, *20*(44), 6270-6272. https://doi.org/10.1038/sj.onc.1204769

Freed-Pastor, W. A., Mizuno, H., Zhao, X., Langerød, A., Moon, S. H., Rodriguez-Barrueco, R., Barsotti, A., Chicas, A., Li, W., Polotskaia, A., Bissell, M. J., Osborne, T. F., Tian, B., Lowe, S. W., Silva, J. M., Børresen-Dale, A. L., Levine, A. J., Bargonetti, J., & Prives, C. (2012). Mutant p53 disrupts mammary tissue architecture via the mevalonate pathway. *Cell*, *148*(1-2), 244-258. https://doi.org/10.1016/j.cell.2011.12.017

Gallagher, E. J., Zelenko, Z., Neel, B. A., Antoniou, I. M., Rajan, L., Kase, N., & LeRoith, D. (2017). Elevated tumor LDLR expression accelerates LDL cholesterol-mediated breast cancer growth in mouse models of hyperlipidemia. *Oncogene*, *36*(46), 6462-6471. https://doi.org/10.1038/onc.2017.247

Göbel, A., Riffel, R. M., Hofbauer, L. C., & Rachner, T. D. (2022). The mevalonate pathway in breast cancer biology. *Cancer Lett*, *542*, 215761. https://doi.org/10.1016/j.canlet.2022.215761

Gong, L., Zhang, D., Lei, Y., Qian, Y., Tan, X., & Han, S. (2018). Transcriptome-wide association study identifies multiple genes and pathways associated with pancreatic cancer. *Cancer Med*, *7*(11), 5727-5732. https://doi.org/10.1002/cam4.1836

Grasso, S., Cangelosi, D., Chapelle, J., Alzona, M., Centonze, G., Lamolinara, A., Salemme, V., Angelini, C., Morellato, A., Saglietto, A., Bianchi, F. T., Cabodi, S., Salaroglio, I. C., Fusella, F., Ognibene, M., Iezzi, M., Pezzolo, A., Poli, V., Di Cunto, F., . . . Defilippi, P. (2020). The SRCIN1/p140Cap adaptor protein negatively regulates the aggressiveness of neuroblastoma. *Cell Death Differ*, *27*(2), 790-807. https://doi.org/10.1038/s41418-019-0386-6

Grasso, S., Chapelle, J., Salemme, V., Aramu, S., Russo, I., Vitale, N., Verdun di Cantogno, L., Dallaglio, K., Castellano, I., Amici, A., Centonze, G., Sharma, N., Lunardi, S., Cabodi, S., Cavallo, F., Lamolinara, A., Stramucci, L., Moiso, E., Provero, P., . . . Defilippi, P. (2017). The scaffold protein p140Cap limits ERBB2-mediated breast cancer progression interfering with Rac GTPase-controlled circuitries. *Nat Commun*, *8*, 14797. https://doi.org/10.1038/ncomms14797

Guerra, B., Recio, C., Aranda-Tavío, H., Guerra-Rodríguez, M., García-Castellano, J. M., & Fernández-Pérez, L. (2021). The Mevalonate Pathway, a Metabolic Target in Cancer Therapy. *Front Oncol*, *11*, 626971. https://doi.org/10.3389/fonc.2021.626971

Guerra, C., Schuhmacher, A. J., Cañamero, M., Grippo, P. J., Verdaguer, L., Pérez-Gallego, L., Dubus, P., Sandgren, E. P., & Barbacid, M. (2007). Chronic pancreatitis is essential for induction of pancreatic ductal adenocarcinoma

by K-Ras oncogenes in adult mice. *Cancer Cell*, *11*(3), 291-302. https://doi.org/10.1016/j.ccr.2007.01.012

Hingorani, S. R., Petricoin, E. F., Maitra, A., Rajapakse, V., King, C., Jacobetz, M. A., Ross, S., Conrads, T. P., Veenstra, T. D., Hitt, B. A., Kawaguchi, Y., Johann, D., Liotta, L. A., Crawford, H. C., Putt, M. E., Jacks, T., Wright, C. V., Hruban, R. H., Lowy, A. M., & Tuveson, D. A. (2003). Preinvasive and invasive ductal pancreatic cancer and its early detection in the mouse. *Cancer Cell*, *4*(6), 437-450. https://doi.org/10.1016/s1535-6108(03)00309-x

Hingorani, S. R., Wang, L., Multani, A. S., Combs, C., Deramaudt, T. B., Hruban, R. H., Rustgi, A. K., Chang, S., & Tuveson, D. A. (2005). Trp53R172H and KrasG12D cooperate to promote chromosomal instability and widely metastatic pancreatic ductal adenocarcinoma in mice. *Cancer Cell*, *7*(5), 469-483. https://doi.org/10.1016/j.ccr.2005.04.023

Honda, H., Oda, H., Nakamoto, T., Honda, Z., Sakai, R., Suzuki, T., Saito, T., Nakamura, K., Nakao, K., Ishikawa, T., Katsuki, M., Yazaki, Y., & Hirai, H. (1998). Cardiovascular anomaly, impaired actin bundling and resistance to Src-induced transformation in mice lacking p130Cas. *Nat Genet*, *19*(4), 361-365. https://doi.org/10.1038/1246

Horton, J. D., Goldstein, J. L., & Brown, M. S. (2002). SREBPs: activators of the complete program of cholesterol and fatty acid synthesis in the liver. *J Clin Invest*, *109*(9), 1125-1131. https://doi.org/10.1172/jci15593

Huang, M., Anand, S., Murphy, E. A., Desgrosellier, J. S., Stupack, D. G., Shattil, S. J., Schlaepfer, D. D., & Cheresh, D. A. (2012). EGFR-dependent pancreatic carcinoma cell metastasis through Rap1 activation. *Oncogene*, *31*(22), 2783-2793. https://doi.org/10.1038/onc.2011.450

Jaworski, J., Kapitein, L. C., Gouveia, S. M., Dortland, B. R., Wulf, P. S., Grigoriev, I., Camera, P., Spangler, S. A., Di Stefano, P., Demmers, J., Krugers, H., Defilippi, P., Akhmanova, A., & Hoogenraad, C. C. (2009). Dynamic microtubules regulate dendritic spine morphology and synaptic plasticity. *Neuron*, *61*(1), 85-100. https://doi.org/10.1016/j.neuron.2008.11.013

Jimenez, C., Hernandez, C., Pimentel, B., & Carrera, A. C. (2002). The p85 regulatory subunit controls sequential activation of phosphoinositide 3-kinase by Tyr kinases and Ras. *J Biol Chem*, *277*(44), 41556-41562. https://doi.org/10.1074/jbc.M205893200

Katoh, K. (2020). FAK-Dependent Cell Motility and Cell Elongation. *Cells*, *9*(1). https://doi.org/10.3390/cells9010192

Koegl, M., Courtneidge, S. A., & Superti-Furga, G. (1995). Structural requirements for the efficient regulation of the Src protein tyrosine kinase by Csk. *Oncogene*, *11*(11), 2317-2329.

Kratimenos, P., Koutroulis, I., Syriopoulou, V., Michailidi, C., Delivoria-Papadopoulos, M., Klijanienko, J., & Theocharis, S. (2017). FAK-Src-paxillin system expression and disease outcome in human neuroblastoma. *Pediatr Hematol Oncol*, *34*(4), 221-230. https://doi.org/10.1080/08880018.2017.1360969

Lamouille, S., Xu, J., & Derynck, R. (2014). Molecular mechanisms of epithelial-mesenchymal transition. *Nat Rev Mol Cell Biol*, *15*(3), 178-196. https://doi.org/10.1038/nrm3758

Lee, T. L., Wang, S. G., Chan, W. L., Lee, C. H., Wu, T. S., Lin, M. L., & Chen, S. S. (2020). Impairment of Membrane Lipid Homeostasis by Bichalcone Analog TSWU-BR4 Attenuates Function of GRP78 in Regulation of the Oxidative Balance and Invasion of Cancer Cells. *Cells*, *9*(2). https://doi.org/10.3390/cells9020371

Li, E., Stupack, D. G., Brown, S. L., Klemke, R., Schlaepfer, D. D., & Nemerow, G. R. (2000). Association of p130CAS with phosphatidylinositol-3-OH kinase mediates adenovirus cell entry. *J Biol Chem*, *275*(19), 14729-14735. https://doi.org/10.1074/jbc.275.19.14729

Li, Y., He, Y., Peng, J., Su, Z., Li, Z., Zhang, B., Ma, J., Zhuo, M., Zou, D., Liu, X., Liu, X., Wang, W., Huang, D., Xu, M., Wang, J., Deng, H., Xue, J., Xie, W., Lan, X., . . . David, C. J. (2021). Mutant Kras co-opts a proto-oncogenic enhancer network in inflammation-induced metaplastic progenitor cells to initiate pancreatic cancer. *Nat Cancer*, *2*(1), 49-65. https://doi.org/10.1038/s43018-020-00134-z

Luo, J., Yang, H., & Song, B. L. (2020). Mechanisms and regulation of cholesterol homeostasis. *Nat Rev Mol Cell Biol*, *21*(4), 225-245. https://doi.org/10.1038/s41580-019-0190-7

Mahammad, S., & Parmryd, I. (2015). Cholesterol depletion using methyl-β-cyclodextrin. *Methods Mol Biol*, *1232*, 91-102. https://doi.org/10.1007/978-1-4939-1752-5_8

Means, A. L., Meszoely, I. M., Suzuki, K., Miyamoto, Y., Rustgi, A. K., Coffey, R. J., Jr., Wright, C. V., Stoffers, D. A., & Leach, S. D. (2005). Pancreatic epithelial plasticity mediated by acinar cell transdifferentiation and generation of nestin-positive intermediates. *Development*, *132*(16), 3767-3776. https://doi.org/10.1242/dev.01925

Miyazaki, T., Zhao, Z., Ichihara, Y., Yoshino, D., Imamura, T., Sawada, K., Hayano, S., Kamioka, H., Mori, S., Hirata, H., Araki, K., Kawauchi, K., Shigemoto, K., Tanaka, S., Bonewald, L. F., Honda, H., Shinohara, M., Nagao, M., Ogata, T., . . . Sawada, Y. (2019). Mechanical regulation of bone homeostasis through p130Cas-mediated alleviation of NF-κB activity. *Sci Adv*, *5*(9), eaau7802. https://doi.org/10.1126/sciadv.aau7802

Moissoglu, K., Kiessling, V., Wan, C., Hoffman, B. D., Norambuena, A., Tamm, L. K., & Schwartz, M. A. (2014). Regulation of Rac1 translocation and activation by membrane domains and their boundaries. *J Cell Sci*, *127*(Pt 11), 2565-2576. https://doi.org/10.1242/jcs.149088

Mollinedo, F., & Gajate, C. (2020). Lipid rafts as signaling hubs in cancer cell survival/death and invasion: implications in tumor progression and therapy: Thematic Review Series: Biology of Lipid Rafts. *J Lipid Res*, *61*(5), 611-635. https://doi.org/10.1194/jlr.TR119000439

Mullen, P. J., Yu, R., Longo, J., Archer, M. C., & Penn, L. Z. (2016). The interplay between cell signalling and the mevalonate pathway in cancer. *Nat Rev Cancer*, *16*(11), 718-731. https://doi.org/10.1038/nrc.2016.76

Navarra, M., Celano, M., Maiuolo, J., Schenone, S., Botta, M., Angelucci, A., Bramanti, P., & Russo, D. (2010). Antiproliferative and pro-apoptotic effects afforded by novel Src-kinase inhibitors in human neuroblastoma cells. *BMC Cancer*, *10*, 602. https://doi.org/10.1186/1471-2407-10-602

Nazih, H., & Bard, J. M. (2020). Cholesterol, Oxysterols and LXRs in Breast Cancer Pathophysiology. *Int J Mol Sci*, *21*(4). https://doi.org/10.3390/ijms21041356

Nick, A. M., Stone, R. L., Armaiz-Pena, G., Ozpolat, B., Tekedereli, I., Graybill, W. S., Landen, C. N., Villares, G., Vivas-Mejia, P., Bottsford-Miller, J., Kim, H. S., Lee, J. S., Kim, S. M., Baggerly, K. A., Ram, P. T., Deavers, M. T., Coleman, R. L., Lopez-Berestein, G., & Sood, A. K. (2011). Silencing of p130cas in ovarian carcinoma: a novel mechanism for tumor cell death. *J Natl Cancer Inst*, *103*(21), 1596-1612. https://doi.org/10.1093/jnci/djr372

Nikonova, A. S., Gaponova, A. V., Kudinov, A. E., & Golemis, E. A. (2014). CAS proteins in health and disease: an update. *IUBMB Life*, *66*(6), 387-395. https://doi.org/10.1002/iub.1282

Omkumar, R. V., & Rodwell, V. W. (1994). Phosphorylation of Ser871 impairs the function of His865 of Syrian hamster 3-hydroxy-3-methylglutaryl-CoA reductase. *J Biol Chem*, *269*(24), 16862-16866.

Paoli, C., & Carrer, A. (2020). Organotypic Culture of Acinar Cells for the Study of Pancreatic Cancer Initiation. *Cancers (Basel)*, *12*(9). https://doi.org/10.3390/cancers12092606

Pawson, T., & Scott, J. D. (1997). Signaling through scaffold, anchoring, and adaptor proteins. *Science*, *278*(5346), 2075-2080. https://doi.org/10.1126/science.278.5346.2075

Payapilly, A., & Malliri, A. (2018). Compartmentalisation of RAC1 signalling. *Curr Opin Cell Biol*, *54*, 50-56. https://doi.org/10.1016/j.ceb.2018.04.009

Pelton, K., Coticchia, C. M., Curatolo, A. S., Schaffner, C. P., Zurakowski, D., Solomon, K. R., & Moses, M. A. (2014). Hypercholesterolemia induces angiogenesis and accelerates growth of breast tumors in vivo. *Am J Pathol*, *184*(7), 2099-2110. https://doi.org/10.1016/j.ajpath.2014.03.006

Radi, M., Brullo, C., Crespan, E., Tintori, C., Musumeci, F., Biava, M., Schenone, S., Dreassi, E., Zamperini, C., Maga, G., Pagano, D., Angelucci, A., Bologna, M., & Botta, M. (2011). Identification of potent c-Src inhibitors strongly affecting the proliferation of human neuroblastoma cells. *Bioorg Med Chem Lett*, *21*(19), 5928-5933. https://doi.org/10.1016/j.bmcl.2011.07.079

Repetto, D., Aramu, S., Boeri Erba, E., Sharma, N., Grasso, S., Russo, I., Jensen, O. N., Cabodi, S., Turco, E., Di Stefano, P., & Defilippi, P. (2013). Mapping of p140Cap phosphorylation sites: the EPLYA and EGLYA motifs have a key role in tyrosine phosphorylation and Csk binding, and are substrates of the

Abl kinase. *PLoS One*, *8*(1), e54931. https://doi.org/10.1371/journal.pone.0054931

Repetto, D., Camera, P., Melani, R., Morello, N., Russo, I., Calcagno, E., Tomasoni, R., Bianchi, F., Berto, G., Giustetto, M., Berardi, N., Pizzorusso, T., Matteoli, M., Di Stefano, P., Missler, M., Turco, E., Di Cunto, F., & Defilippi, P. (2014). p140Cap regulates memory and synaptic plasticity through Src-mediated and citron-N-mediated actin reorganization. *J Neurosci*, *34*(4), 1542-1553. https://doi.org/10.1523/jneurosci.2341-13.2014

Riggins, R. B., DeBerry, R. M., Toosarvandani, M. D., & Bouton, A. H. (2003). Src-dependent association of Cas and p85 phosphatidylinositol 3'-kinase in v-crk-transformed cells. *Mol Cancer Res*, *1*(6), 428-437.

Rodgers, W., & Rose, J. K. (1996). Exclusion of CD45 inhibits activity of p56lck associated with glycolipid-enriched membrane domains. *J Cell Biol*, *135*(6 Pt 1), 1515-1523. https://doi.org/10.1083/jcb.135.6.1515

Rovero, S., Amici, A., Di Carlo, E., Bei, R., Nanni, P., Quaglino, E., Porcedda, P., Boggio, K., Smorlesi, A., Lollini, P. L., Landuzzi, L., Colombo, M. P., Giovarelli, M., Musiani, P., & Forni, G. (2000). DNA vaccination against rat her-2/Neu p185 more effectively inhibits carcinogenesis than transplantable carcinomas in transgenic BALB/c mice. *J Immunol*, *165*(9), 5133-5142. https://doi.org/10.4049/jimmunol.165.9.5133

Salemme, V., Angelini, C., Chapelle, J., Centonze, G., Natalini, D., Morellato, A., Taverna, D., Turco, E., Ala, U., & Defilippi, P. (2021). The p140Cap adaptor protein as a molecular hub to block cancer aggressiveness. *Cell Mol Life Sci*, *78*(4), 1355-1367. https://doi.org/10.1007/s00018-020-03666-w

Sawada, Y., Tamada, M., Dubin-Thaler, B. J., Cherniavskaya, O., Sakai, R., Tanaka, S., & Sheetz, M. P. (2006). Force sensing by mechanical extension of the Src family kinase substrate p130Cas. *Cell*, *127*(5), 1015-1026. https://doi.org/10.1016/j.cell.2006.09.044

Schlaepfer, D. D., Broome, M. A., & Hunter, T. (1997). Fibronectin-stimulated signaling from a focal adhesion kinase-c-Src complex: involvement of the Grb2, p130cas, and Nck adaptor proteins. *Mol Cell Biol*, *17*(3), 1702-1713. https://doi.org/10.1128/mcb.17.3.1702

Sezgin, E., Levental, I., Mayor, S., & Eggeling, C. (2017). The mystery of membrane organization: composition, regulation and roles of lipid rafts. *Nat Rev Mol Cell Biol*, *18*(6), 361-374. https://doi.org/10.1038/nrm.2017.16

Sharma, N., Repetto, D., Aramu, S., Grasso, S., Russo, I., Fiorentino, A., Mello-Grand, M., Cabodi, S., Singh, V., Chiorino, G., Turco, E., Stefano, P. D., & Defilippi, P. (2013). Identification of two regions in the p140Cap adaptor protein that retain the ability to suppress tumor cell properties. *Am J Cancer Res*, *3*(3), 290-301.

Skočaj, M., Bakrač, B., Križaj, I., Maček, P., Anderluh, G., & Sepčić, K. (2013). The sensing of membrane microdomains based on pore-forming toxins. *Curr Med Chem*, *20*(4), 491-501. https://doi.org/10.2174/0929867311320040002

Stefely, J. A., & Pagliarini, D. J. (2017). Biochemistry of Mitochondrial Coenzyme Q Biosynthesis. *Trends Biochem Sci*, *42*(10), 824-843. https://doi.org/10.1016/j.tibs.2017.06.008

Storz, P. (2017). Acinar cell plasticity and development of pancreatic ductal adenocarcinoma. *Nat Rev Gastroenterol Hepatol*, *14*(5), 296-304. https://doi.org/10.1038/nrgastro.2017.12

Storz, P., & Crawford, H. C. (2020). Carcinogenesis of Pancreatic Ductal Adenocarcinoma. *Gastroenterology*, *158*(8), 2072-2081. https://doi.org/10.1053/j.gastro.2020.02.059

Tikhmyanova, N., Little, J. L., & Golemis, E. A. (2010). CAS proteins in normal and pathological cell growth control. *Cell Mol Life Sci*, *67*(7), 1025-1048. https://doi.org/10.1007/s00018-009-0213-1

Tomasoni, R., Repetto, D., Morini, R., Elia, C., Gardoni, F., Di Luca, M., Turco, E., Defilippi, P., & Matteoli, M. (2013). SNAP-25 regulates spine formation through postsynaptic binding to p140Cap. *Nat Commun*, *4*, 2136. https://doi.org/10.1038/ncomms3136

Tornillo, G., Bisaro, B., Camacho-Leal Mdel, P., Galiè, M., Provero, P., Di Stefano, P., Turco, E., Defilippi, P., & Cabodi, S. (2011). p130Cas promotes invasiveness of three-dimensional ErbB2-transformed mammary acinar structures by enhanced activation of mTOR/p70S6K and Rac1. *Eur J Cell Biol*, *90*(2-3), 237-248. https://doi.org/10.1016/j.ejcb.2010.09.002

Tornillo, G., Defilippi, P., & Cabodi, S. (2014). Cas proteins: dodgy scaffolding in breast cancer. *Breast Cancer Res*, *16*(5), 443. https://doi.org/10.1186/s13058-014-0443-5

Touvier, M., Fassier, P., His, M., Norat, T., Chan, D. S., Blacher, J., Hercberg, S., Galan, P., Druesne-Pecollo, N., & Latino-Martel, P. (2015). Cholesterol and breast cancer risk: a systematic review and meta-analysis of prospective studies. *Br J Nutr*, *114*(3), 347-357. https://doi.org/10.1017/s000711451500183x

Vona, R., Iessi, E., & Matarrese, P. (2021). Role of Cholesterol and Lipid Rafts in Cancer Signaling: A Promising Therapeutic Opportunity? *Front Cell Dev Biol*, *9*, 622908. https://doi.org/10.3389/fcell.2021.622908

Wang, Y., Zhou, X., Lei, Y., Chu, Y., Yu, X., Tong, Q., Zhu, T., Yu, H., Fang, S., Li, G., Wang, L., Wang, G. Y., Xie, X., & Zhang, J. (2022). NNMT contributes to high metastasis of triple negative breast cancer by enhancing PP2A/MEK/ERK/c-Jun/ABCA1 pathway mediated membrane fluidity. *Cancer Lett*, *547*, 215884. https://doi.org/10.1016/j.canlet.2022.215884

Waters, A. M., Khatib, T. O., Papke, B., Goodwin, C. M., Hobbs, G. A., Diehl, J. N., Yang, R., Edwards, A. C., Walsh, K. H., Sulahian, R., McFarland, J. M., Kapner, K. S., Gilbert, T. S. K., Stalnecker, C. A., Javaid, S., Barkovskaya, A., Grover, K. R., Hibshman, P. S., Blake, D. R., . . . Der, C. J. (2021). Targeting p130Cas- and microtubule-dependent MYC regulation sensitizes pancreatic cancer to ERK MAPK inhibition. *Cell Rep*, *35*(13), 109291. https://doi.org/10.1016/j.celrep.2021.109291

Wei, Y., Huang, Y., Yang, W., Huang, Q., Chen, Y., Zeng, K., Chen, J., & Chen, J. (2021). The significances and clinical implications of cholesterol components in human breast cancer. *Sci Prog*, *104*(3), 368504211028395. https://doi.org/10.1177/00368504211028395

Wolpin, B. M., Rizzato, C., Kraft, P., Kooperberg, C., Petersen, G. M., Wang, Z., Arslan, A. A., Beane-Freeman, L., Bracci, P. M., Buring, J., Canzian, F., Duell, E. J., Gallinger, S., Giles, G. G., Goodman, G. E., Goodman, P. J., Jacobs, E. J., Kamineni, A., Klein, A. P., . . . Amundadottir, L. T. (2014). Genome-wide association study identifies multiple susceptibility loci for pancreatic cancer. *Nat Genet*, *46*(9), 994-1000. https://doi.org/10.1038/ng.3052

Xue, L., Qi, H., Zhang, H., Ding, L., Huang, Q., Zhao, D., Wu, B. J., & Li, X. (2020). Targeting SREBP-2-Regulated Mevalonate Metabolism for Cancer Therapy. *Front Oncol*, *10*, 1510. https://doi.org/10.3389/fonc.2020.01510

Yamauchi, M., Sudo, K., Ito, H., Iwamoto, I., Morishita, R., Murai, T., Kajita, K., Ishizuka, T., & Nagata, K. (2013). Localization of multidomain adaptor proteins, p140Cap and vinexin, in the pancreatic islet of a spontaneous diabetes mellitus model, Otsuka Long-Evans Tokushima Fatty rats. *Med Mol Morphol*, *46*(1), 41-48. https://doi.org/10.1007/s00795-013-0008-1

Zeisig, R., Koklic, T., Wiesner, B., Fichtner, I., & Sentjurc, M. (2007). Increase in fluidity in the membrane of MT3 breast cancer cells correlates with enhanced cell adhesion in vitro and increased lung metastasis in NOD/SCID mice. *Arch Biochem Biophys*, *459*(1), 98-106. https://doi.org/10.1016/j.abb.2006.09.030

Zhao, W., Prijic, S., Urban, B. C., Tisza, M. J., Zuo, Y., Li, L., Tan, Z., Chen, X., Mani, S. A., & Chang, J. T. (2016). Candidate Antimetastasis Drugs Suppress the Metastatic Capacity of Breast Cancer Cells by Reducing Membrane Fluidity. *Cancer Res*, *76*(7), 2037-2049. https://doi.org/10.1158/0008-5472.Can-15-1970